POLITECNICO DI TORINO

Master's degree in Aerospace Engineering

Thesis

Topological optimization of a drone propeller using commercial CFD code

Supervisor:
Prof. Francesco LAROCCA

Candidate:
Luca RAIOLA

Co-Supervisor:
Prof. Domenic D'AMBROSIO

Agom Tutor:
Eng. Fabio ZAMBONI

Academic Year 2019-2020

POLITECNICO
DI TORINO

Dipartimento
di Ingegneria Meccanica
e Aerospaziale

AGOM

Politecnico di Torino

Master's degree in Aerospace Engineering

Thesis

Topological optimization of a drone propeller using commercial CFD code

Supervisor:
Prof. Francesco LAROCCA

Candidate:
Luca RAIOLA

Co-Supervisor:
Prof. Domenic D'AMBROSIO

Agom Tutor:
Eng. Fabio ZAMBONI

Academic Year 2019-2020

To my beloved parents.

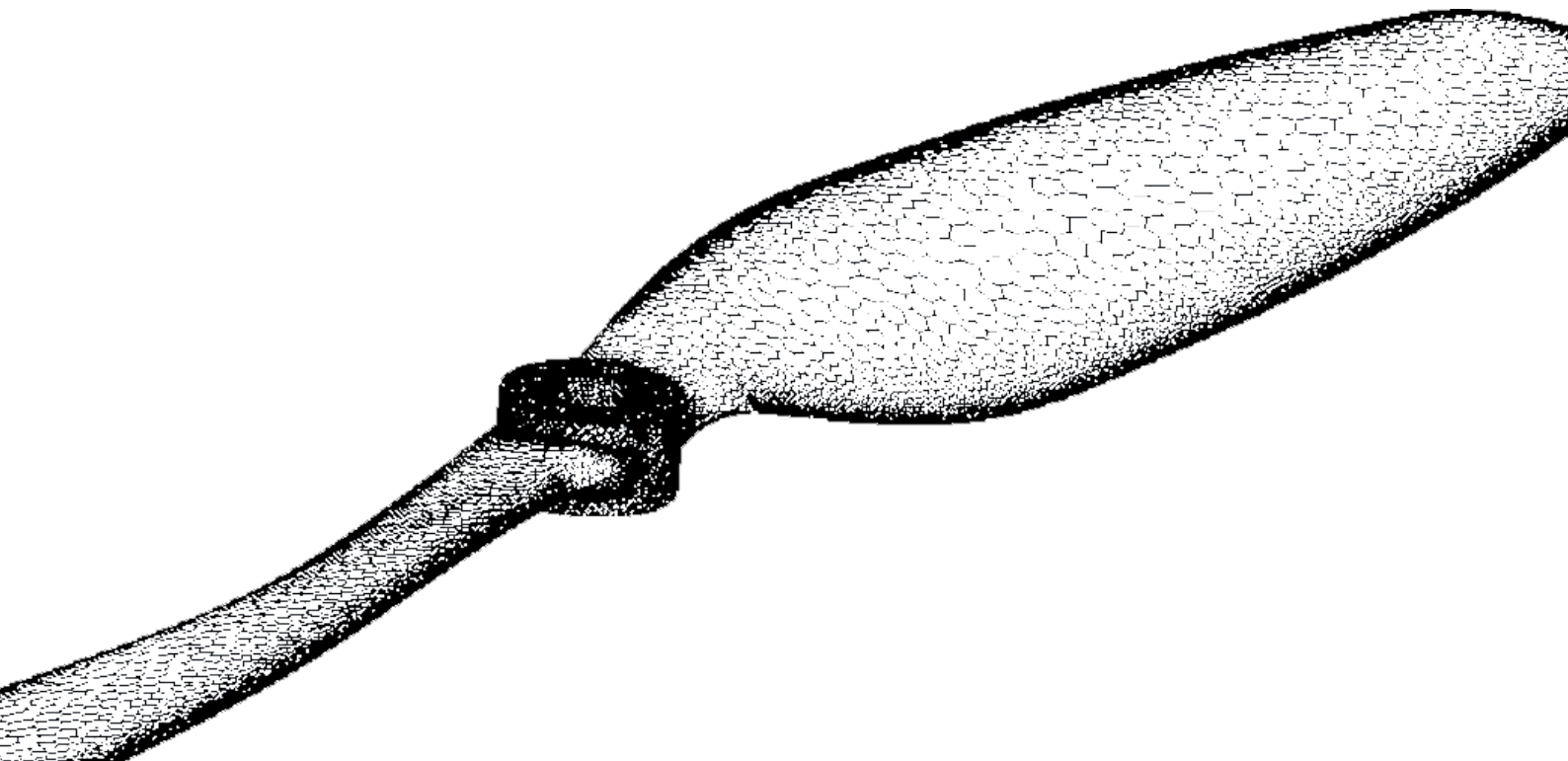

Abstract

This thesis was born as a first step of a bigger project aimed at characterizing and studying a drone propeller to optimize the geometry to achieve a greater efficiency and therefore longer life of multirotors adopts these propellers. Being a very large project that aims to achieve advanced optimization also by studying the flight envelope of a typical multirotor mission, it was necessary to start from a basic level to create the foundations of what will be the future work and gain confidence of the work process.

In this paper, the objective was to study a propeller used for the propulsion of multirotors. After having dealt with some fundamental notions to understand *propeller* and to share some basis of *Computational Fluid Dynamics*, it is continued towards the heart of the thesis.

The central part of the dissertation deals with some types of analysis made to study the object under examination, the propeller was designed a parametric propeller with CAD software and it is transferred into the resolution program of the fluid-dynamic equations *STAR CCM +*.

A good part of the thesis concerns the study of the mesh to ensure the confidence of the case study and better manage a future simulation with the entire propeller. Parallel to the study of the optimal mesh in terms of size of the rotating domain and number of layers of the prism layer, the first results were obtained on the propeller for design conditions. The mesh obtained was also validated by comparing the results obtainable with those of a propeller whose performance was known.

Finally, the propeller was studied with a simple 2D process to try to improve the starting propeller, this was then analyzed manually through a simulation campaign aimed at finding, by changing the keying angle, the geometry that would return a maximum thrust room.

Sommario

Questa tesi è nata come primo passo per un progetto più grande volto a caratterizzare e studiare un elica di un drone per poter ottimizzarne la geometria affinchè si abbia una maggior efficienza e quindi maggior durata del multirotore che adotta tali eliche. Essendo un progetto molto ampio che si pone l'obiettivo di raggiungere un ottimizzazione avanzata anche studiando l'inviluppo di volo di una missione tipica del multirotore, è stato necessario partire da un livello base per creare le fondamenta di quello che sarà il lavoro futuro e ottenere confidenza del processo lavorativo.
In questo elaborato ci si è posto come obiettivo quello di andare a studiare un elica utilizzata per la propulsione di multirotori. Dopo aver trattato alcune nozioni fondamentali per capire l'argomento *elica* e per avere una base di *fluidodinamica computazionale* si è proseguito verso il cuore della tesi.
La parte centrale della dissertazione tratta alcuni tipi di analisi fatti per studiare l'oggetto in esame, l'elica è stata progettata parametricamente con software CAD ed è trasferita nel programma di risoluzione delle equazioni fluidodinamiche STAR CCM +. Una buona parte della tesi riguarda lo studio della mesh per garantire la confidenza del caso di studio e gestire meglio una futura simulazione con l'intera elica. Parallelamente allo studio della mesh ottimale in termini di dimensioni del dominio rotante e numero di strati del prism layer sono stati ricavati i primi risultati sull'elica per condizioni di progettazione. E' stata inoltre validata la mesh ottenuta confrontando i risultati ottenibili con quelli di un elica le cui performance fossero note.
Infine, è stata studiata l' elica con un semplice processo 2D per cercare migliorare l'elica di partenza , questa è stata quindi analizzata manualmente attraverso una campagna di simulazioni volta a trovare, modificando l'angolo di calettamento, la geometria che restituisse un massimo locale della spinta.

Contents

List of Figures

Chapter 1

Introduction

Talking about aircraft is possible to discern in two main families, the most spread and used for commercial transport of people and goods are fixed wing aircraft, then to the other side are rotorcraft.
Rotorcrafts are aircrafts using rotating blades for generate lift even in absence of forward airspeed, in contrast to fixed wing, which need horizontal velocity to sustain flight.
This feature allows the rotorcraft to hover and take off and land without the need of large space, so nearly from everywhere.

1.1 Helicopter

The most common rotorcrafts are the helicopter, these are aircrafts with rotor blades rotates around vertical axis describing a disk in nearly horizontal plane. The blades generate the aerodynamic forces through the relative air motion on itself. These forces can be generated even if there isn't horizontal velocity of rotorcraft.
For conventional helicopter the torque created by the main rotor has countered by another moment produced by a blade rotates around horizontal axis, also providing yaw control and directional stability.

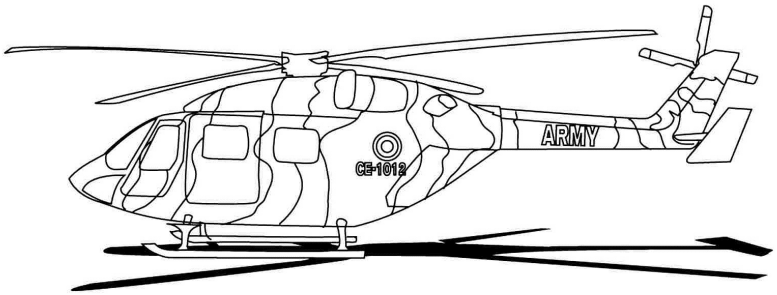

Figure 1.1: Standard helicopter

Nowadays are available different vehicles from conventional helicopter, these instead were built using different solution like other rotor and even auxiliary devices and wings to alleviate some of propulsion or lifting requirements.
In conventional helicopter, the hovering is accomplished by the thrust force opposing the rotorcraft weight, so efficient vertical flight is described by low ratio of rotor power required to rotor thrust, called disk loading, because the fuel consumption of aircraft is proportional to the power required.
Through conservation of momentum is possible to see that the rotor lift is obtained by accelerating air downward to generate an equal and opposite reaction of the rotating blades against air that is called lift.
The disk loading characteristic of helicopter is in range of 100 to 500 $\frac{N}{m^2}$, so they uses the lowest value of disk loading of all Vertical Take Off and Landing *VTOL* vehicle, but they has the most efficient vertical flight capability.
The horizontal flight is allowed, for low speeds, by manage blades cyclic tilt producing on the disk a zone with higher lift than average on disk. The negative side of rotorcraft is the higher power requirement compared to fixed wing

and the elevated cost for building helicopter and maintenance.

1.2 Drone

The technological advancement and electric motors permit to create the most known Unmanned Aerial Vehicle *UAV* of nowadays.
At first they were created for military bombing mission, through time they are changed from simple air balloon to aircraft capable of flying over a target, accomplish their own mission and safely come back to base, without any risk for human lives thanks to remote control. There are two principal families of drone

- **Fixed wing**
  Look like airplanes, they have generally one or two propulsive system and the lift generation is performed through aerodynamic fixed surfaces. Besides normal airplane, this type of drone does not carry any human so they can be built to withstand an higher load factor and usually, like the Reaper 1.2 are built for military intent like surveillance of hot spot.

Figure 1.2: Reaper Drone

- **Rotary wing**
  Multirotors drone usually used in civil sphere, like helicopter they are *VTOL* aircraft. Exploiting a complex flight control system, they can manage the rotation speed of each propeller, which it generates thrust and so regulate attitude and altitude of itself 1.3.

Figure 1.3: Multirotor Drone

1.2.1 Components

Focusing on rotary wing drone, subject of this thesis, is interesting decompose it to see how it is made

- **Receiver**
  This use radio wave to receive flight controls from pilot and then transmit it to flight control unit.

- **GPS e IMU**
  Used by the drone to understand is position and attitude in the space. GPS and integrate magnetometer are needed to obtain the direction

and position, besides the Inertial Measurement Unit return the attitude respect the ground.

- **Battery and PDB**
  This is the drone power management system, the battery is connected to a Power Distribution Board, that will split the power from battery to all systems of drone.

- **ESC**
  Electronic Speed Control, they manage the current and signals received and transform it into a three phase output used to regulate the rotation speed of motors and linked propellers.

- **Flight Controller**
  The core of the drone, elaborate the sensors and pilot signal to generate signal for ESCs to keep the attitude of drone or handle its movement.

- **Frame**
  The structure of drone, has a crucial role because is the only component that resist stresses due by propellers thrust torque in take off, landing or impact. Usually made of different materials like plastic, aluminium or carbon fiber composite.

- **Motors**
  This component receive signal from ESCs and power from the PDB and rotates an axes in function of signal received. Can be brush motor or more spread three phase brushless motors more reliable and generate more torque.

- **Propellers**
  At last the most important components, these convert motors torque into thrust by aerodynamics forces on its rotating surfaces.

Multirotor drones usually has three or more rotors, the reasons for this can be traced to redundancy needs and improving lift capabilities keeping small volume dimensions.
On the other hand this type of drones needs complex controls for manage lift and rotating the entire rotorcraft through increasing all or differential rotors speed.

1.2.2 Deepening on the Propellers

Propellers are a type of fan that converts mechanical energy in kinetic energy of the fluid. The momentum increment of the fluid generates the thrust.
Below are listed propeller's parameters

- **Velocity**
  Incoming fluid velocity and rotation velocity determines the pitch distribution of propeller. For example a large pitch propellers may have a good efficiency at design point, but can have problems they have to work on axial velocity ending up to stall.

- **Number of blades**
  This parameter has a small effect on efficiency. Usually a propeller with more blades will perform slightly better, thanks to more evenly power and thrust distribution in its wake.

- **Diameter**
  Propeller diameter has a big influence on performance. Usually larger propeller will have a higher efficiency, as it catches more incoming fluid and so distributes its power and thrust on a larger fluid volume.

- **Fluid Density**
  Density of fluid has no influence on the efficiency of a propeller, but has

a strong impact on size and shape. This happens because the forces and the power are directly proportional to fluid density. An example is hydro propeller that has much smaller dimensions than a propeller working in air. Is important to remember that the tip sections of propellers operating at Mach numbers near to 0.7, so should be designed to has a small lift coefficient below 0.5.

- **Lift and Drag distribution**
  The distribution of C_L and C_D along the radius can be examined by performing an analysis for the design point. Maximum performance can be obtain if airfoils operate at maximum L/D. Moreover, propellers are designed with lower angle of attack to always work in good conditions.

Propeller design parameters

Propeller blade is a crucial part of drone because as rotating airfoil they produces lift and drag.It has both induced downwash and upwash due to complex helical trailing vortices that it generates. The two most important performance parameters of propeller design and analysis are torque and thrust it produces. The propeller blade generate thrust (T) and torque (Q) that can be represent (1.4) as

$$dT = dLcos(\phi + \alpha_i) - dDsin(\phi + \alpha_i) \tag{1.1}$$

$$dQ = r[dLsin(\phi + \alpha_i) + dDcos(\phi + \alpha_i)] \tag{1.2}$$

$$dL = \frac{1}{2}\rho V_e^2 c C_L d \tag{1.3}$$

$$dD = \frac{1}{2}\rho V_e^2 c C_D r d \tag{1.4}$$

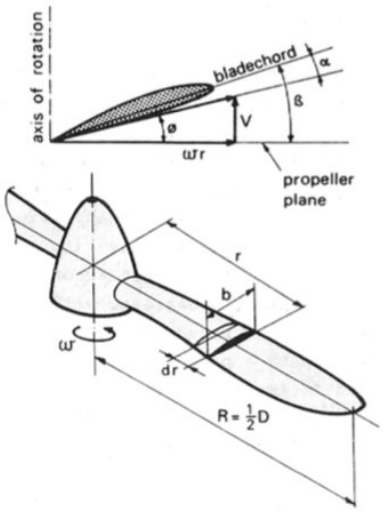

Figure 1.4: Propeller blade element and local direction of flow [6]

Propeller materials

For manufacturing propellers usually are used the following materials

- **Aluminium**
  Aluminium has a Young modulus of 69 GPa, is the most popular material for marine propeller. It is cheap and has a good strength.

- **Stainless steel**
  Stainless steel has a Young modulus of 200 GPa and is strongest and most durable material of material used for outboard and stern drive propellers. To drone application can be made thinner that returns even better efficiency.

- **Plastic and Composite material**
  Plastic and composite material propellers flex considerably under high loads, light and cheap are a good solution for drone propeller. Young modulus has a wide range of values due the type of plastic or fiber orientation.

- **Wood**
  Generally common wood has a Young modulus near 10 GPa, cheap and easy to substitute is a good initial choice to test propeller design.

Other materials can be used for the production of propellers, the choice is only due to the type of application for those propellers.

1.2.3 Reference legislation

Historically talking, drones are quite recent, but due their huge possibilities there is need to standardize and categorize them. This work was made by *ENAC* (Ente Nazionale per l'Aviazione Civile) it is the Italian authority about technical regulation, certification and surveillance in civil aviation.
ENAC follow step by step EASA (European Aviation Safety Agency), for this thesis is analyzed the last amendment for Remote control aircrafts on ENAC.

The Fourth Amendment of 21 June 2018 analyzed amendment starts delineate the difference the Remote Pilot Aircrafts (SAPR Sistemi Aeromobili a Pilotaggio Remoto), the categorization is function of take off operative mass and there is a threshold of 25 kg and a maximum weight limit of 150 kg. About their use drones are distinguish by specialized operation and research and development activities.

SAPR with take off operative mass less than 25 kg

Article 8 of amendment rules on general requirements for SAPR use. Inside there are principal rules for who own and want to use an aircraft that be part of aforementioned category. Most important are the need of obtain a flight manual, the equipment for live stream of SAPR data and the duty from pilot of SAPR to have the recognition of the competence to pilot the vehicle. Is possible to distinguish the type of operation

- **No Critical Operations**, leads in VLOS (Visual Line of Sight) that does not expect urban or sensible infrastructure overfly.
- **Critical Operations**, these does not respect even partially the previous description, for these is imperative to obtain an authorization and insurance of determined security level.

SAPR with take off operative mass equal or over than 25 kg

In this case is mandatory the registration of drone and the release of a Flight Permit for the SAPR, obtainable only for research and development goal or specialized operations without a Restricted Type Certification.
In case of Restricted Type Certification ownership is needed to obtain a Restricted Navigability Certificate too, released after a owner's presentation of a constructor declaration that the SAPR is accordant to the certificate. Here the possible operations are not differentiated, but even here the pilot need a maintenance schedule correlated to ensure the maintenance of the airworthiness of system.

Figure 1.5: Cover of the EASA summary of drones

Chapter 2

Propellers

The propeller is a type of fan that converts mechanical energy into thrust power by accelerating the propulsive fluid. Propeller dynamics can be modelled by Bernoulli's principle and Newton's third law.
Propellers can be distinguish into two type

- Fixed Pace
  During movement the propeller's pace rim cannot change. To modify thrust of propeller need to operate on angular velocity of propeller. These are used in drones.

- Constant turns
  Thrust change with propeller rim at constant speed.

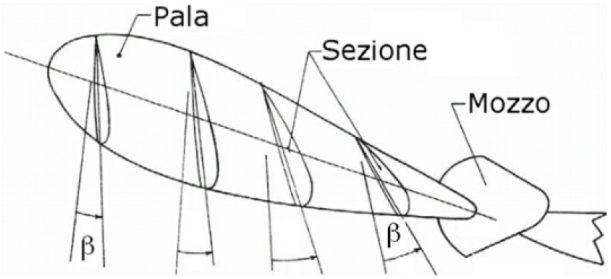

Figure 2.1: Propeller Section and twist [8]

2.1 Propeller parameters

2.1.1 Pace and twist

Propeller parameters conventionally are taken at 75% of prop length. Looking at 2.1 you can see the rim angle β is bigger at root of prop, as the velocity V is constant the $\omega \cdot r$ decrease so as α angle of attack. Instead to the tip for avoid stall effect β is reduced.
The twist law of propeller will be studied to optimize the performance.

$$p = 2\pi r tan\beta \neq \textbf{cost} \tag{2.1}$$

Using 2.1 can be defined the twist law of propeller along the radius.

2.1.2 θ angle

This angle is used to describe the progress report J

$$J = tan\theta = \frac{V}{\omega r} \tag{2.2}$$

This is a characteristic parameter of propeller behaviour, that can be used

- With ω =cost, changing flight attitude to change V
- With V =cost, changing the throttle

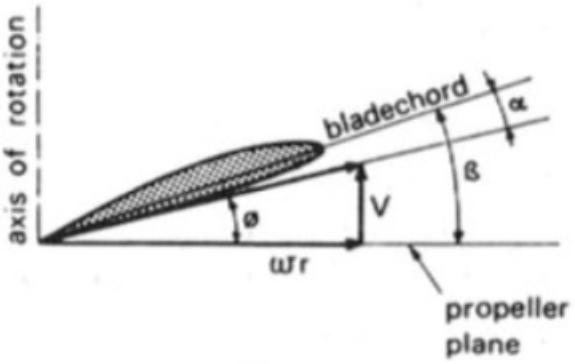

Figure 2.2: Propeller section [8]

Usually with a Fixed Pace propeller are both modified instead with a Constant turns propeller only V is altered.

2.1.3 Angle of attack $\alpha = \beta - \theta$

Varying *alpha* the propeller disk change the own thrust. In aeronautic the propeller's operation range is quite shrink, so the angle of attack is very important parameter, instead for aeromodelling or drone application is possible to increase a lot the angular velocity of propeller reducing substantially θ at same β.

The maximum of thrust, at which the angle of attack is maximum, is at fixed point $V = 0 \rightarrow \theta = 0$ When the propeller disk is moving it as to add the velocity V that change θ until $\theta \simeq \beta$ leading to $\alpha \sim 0$ equal to a negligible thrust, this is named J_1. After this progress report the propeller disk became braking. With fixed pace propeller velocity V can move from 0 to J_1 strongly limiting us specially if are requested highly cruise velocity.

Because of that have been created constant turns propeller, to expand operation range, this leads to another limit that is the torque, increasing β drive to a bigger C_D, so usually angle of attack tend to a the value that returns the maximum efficiency E.

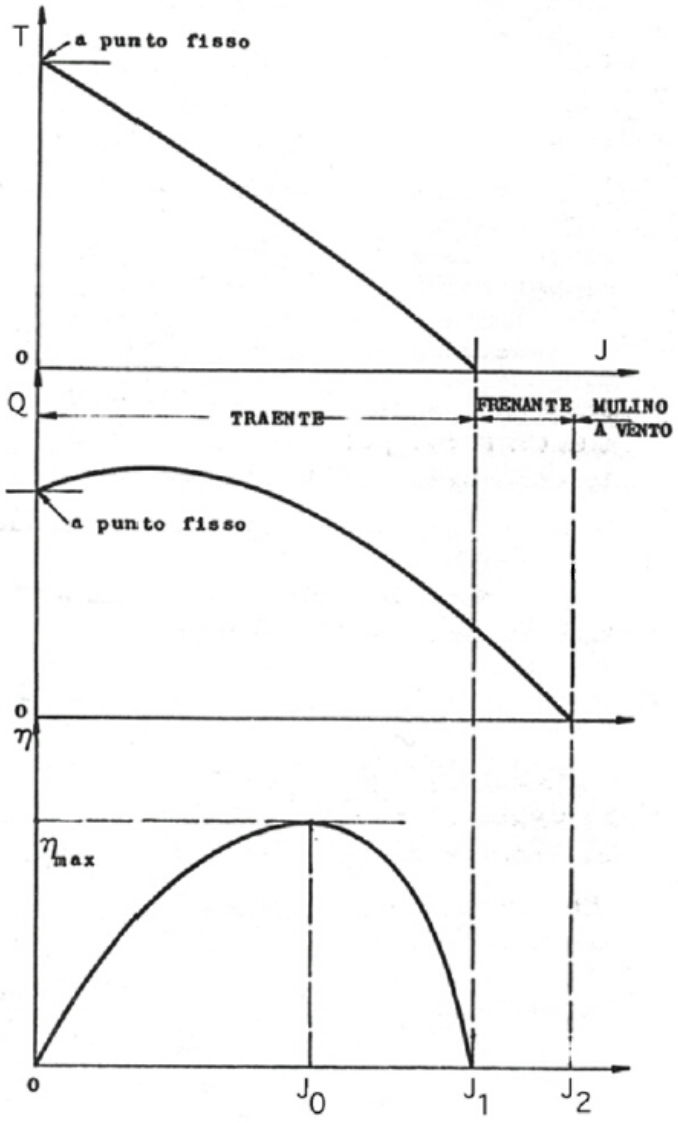

Figure 2.3: Propeller Thrust, Torque and Efficiency with progress report[8]

In 2.3 is interesting to see the J_2 value to which the torque is equal to zero and the engine start to rotate dragged by the air to over speed state.

Chapter 3

Impulsive Theories

3.1 Actuator Disk principle

Aerodynamic analysis of propellers lead to problems due complexity of system, to accomplish complete investigation it has to consider a instationary, compressible and viscous flowfield around complex shapes.
Similarly to Prandtl lifting line theory, this theory neglects the flowfield nearly the body, that allows to look at the propeller as infinitesimal thickness, so from now on the propeller will be modeled as a discontinuity surface.
Replacing the real rotor with a permeable disk with same area, but the forces are distributed on circular disk and were generated by stationary, non viscous and incompressible flow with V_∞ velocity normal to the disk, introducing a pressure gap 3.1.

These distributed forces on the actuator disk transform the local velocities in the entire flowfield. The flowfield is driven by Euler's equation of motion, mass conservation law and the balance of momenta, which for real rotor is given by the axial and tangential momentum equation.
Furthermore energy of flow upstream and downstream the disk is different, applying energy conservation equation it can be found that the difference is

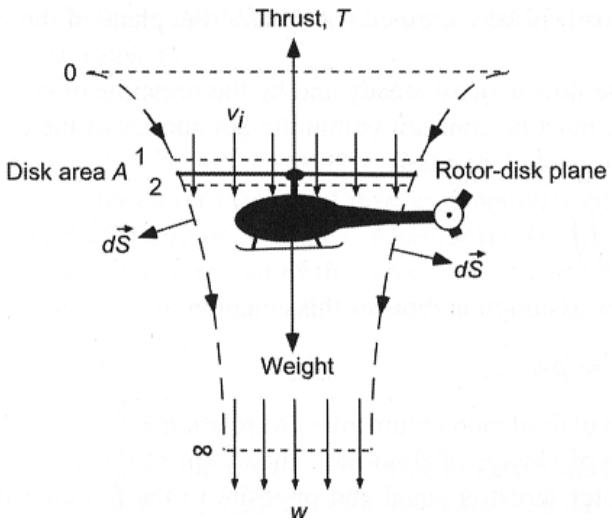

Figure 3.1: Actuator disk scheme

equal to expense power, this can form a contact discontinuity called propeller wake.

The balance of momenta can be written using p' and $p' + \Delta p$ for each average pressure upstream and downstream of disk integrating on the volume enclosed by S_∞ surface that contain the entire flowfield and A area of actuator disk.

$$\int_{S_\infty} (p\bar{\bar{I}} + \rho \bar{V}\bar{V}) \cdot \bar{n} dS - \Delta p A \bar{k} = 0 \tag{3.1}$$

With $\bar{n}$ outgoing normal versor from surface S_∞ and $\bar{k}$ versor aligned with V_∞. The thrust on disk is given by the pressure gap multiplied actuator disk area

$$T = \Delta p A = \bar{k} \dot{\int}_{S_\infty} (p\bar{\bar{I}} + \rho \bar{V}\bar{V}) \cdot \bar{n} dS \tag{3.2}$$

Mass conservation law defines mass flow through flow tube

$$\dot{m} = \rho V_\infty A_u = \rho V_d A_d \tag{3.3}$$

Using d subscript denoting average quantities inside downstream disk wake, although u subscript is for upstream.

Decomposing the surface S_∞ with the sections upstream, downstream and lateral

$$T = \bar{k} \cdot \int_{\S_{\infty ext}} [(p - p_\infty)\bar{n} + \rho \bar{V}\bar{V} \cdot \bar{n}]dS + \dot{m}(V_d - V_\infty) + (p_d - p_\infty)A_d \quad (3.4)$$

The last equation is null because lateral surface at infinite $S_{\infty ext}$ can be assumed as surface where there isn't crossing flow momentum.
Even the pressure term gives null contribute since this is order of $\frac{1}{r^2}$. Last term can be non equal to zero considering in disk wake may be present some rotational terms, they imply bearing of a pressure gradient.

$$T = \dot{m}(V_d - V_\infty) + (p_d - p_\infty)A_d \quad (3.5)$$

3.2 Simple momentum theory

Developed by Rankine during half of eight century, the simple impulsive theory grant physical quantities inside flow tube be only z function.
It can be assumed that through disk there isn't discontinuity of tangential velocity component, so it doesn't generate flow rotation, translatable as cancelling pressure term downstream the wake.

Applying fundamental laws of fluid dynamics it can be used for ideal performance of rotor, is important to remember that is not allowed determination of flow field nearly around propeller neither the distributed forces on it.
Instead this theory can be used quite well for long distance from propeller flow field determination.
The hypothesis used for the theory

- Stationary and irrotational flow.
- Ideal flow (incompressible and non viscous)
- Velocity and pressure gaps are constant along disk radius

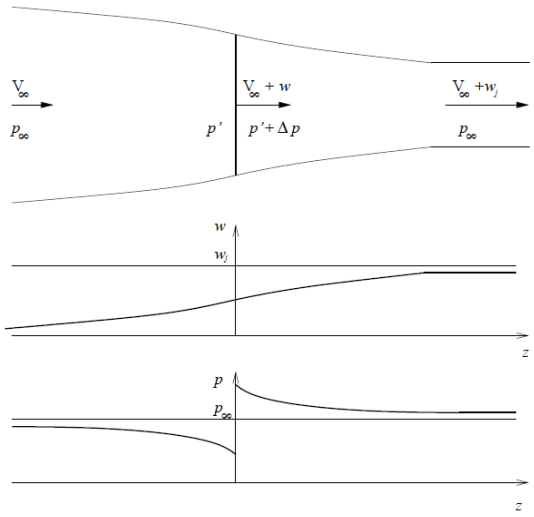

Figure 3.2: Simple momentum theory actuator disk scheme [1]

As shown on 3.2 flow velocity does not has discontinuity, rather the disk introduce a pressure gap. Tangential term of velocity is null because the irrotational of flow, the radius term is negligible so the flow field induced from simple actuator disk is axial symmetric.

Employing Bernoulli theorem to upstream and downstream flow tube and subtracting them

$$\Delta p = \rho\omega_d(V_\infty + \frac{1}{2}\omega_d) \tag{3.6}$$

Instead, using (3.2) and (3.5)

$$\Delta p = \rho\omega_d(V_\infty + \omega) \tag{3.7}$$

By comparison is obtained that induction downstream is double induction on disk

$$\omega = \frac{1}{2}\omega_d \tag{3.8}$$

The thrust can be written as

$$T = \int_{A_d} \Delta p \cdot dA = \int_0^{R_d} \Delta p \cdot 2\pi r dr \tag{3.9}$$

With an uniform pressure gap (3.9) becomes

$$T = \Delta p \cdot A_d = 2\rho A_d(V_\infty + \omega) \tag{3.10}$$

For a propulsive propeller the velocity raise and the flow tube as to contract as shown as 3.2. The needed power to obtain that thrust can be evaluated by kinetic energy change of flow

$$P = \dot{m}[\frac{1}{2}(V_\infty + \omega_d)^2 - \frac{1}{2}V_\infty^2] = T(V_\infty + \omega) \tag{3.11}$$

The performance can be written using $a = \frac{\omega}{V_\infty}$ called axial interference factor

$$\eta = \frac{TV_\infty}{P} = \frac{1}{1+a} \tag{3.12}$$

Equation (3.12) gives an important project criteria: to obtain the maximum propeller efficiency, the axial interference factor must be as smaller as possible, so it has to be used the maximum possible diameter.

3.2.1 Hovering

Hovering status denoting a vertical flight where the rotor maintain it's altitude and the infinity upstream velocity of tube flow is null. Static equilibrium at vertical translation must place thrust equal to weight: $T = W$.
Simple actuator disk theory's results are still valid with a simplification

$$T = \frac{\pi}{2}\rho D_d^2 \omega^2 \tag{3.13}$$

$$\Delta p = 2\rho\omega^2 \tag{3.14}$$

With ω inducted velocity on disk and D_d the disk diameter. Moreover using differential thrust definition

$$dT = 4\pi r \rho \omega^2 dr \tag{3.15}$$

3.3 Extended momentum theory

Simple momentum theory can be extended including downstream wake rotation and associate loss. In this theory is still neglected wake contraption caused by u velocity, this can be done assuming $u = O(\omega^2)$, but ω and v as the same order of magnitude.
Once more is assumed stationary, non viscous and incompressible flow, but this time is a rotational flow. The goal of theory is to obtain axial and tangential disk velocities that lead to minimum inducted power at fixed thrust.

As shown on 3.3 $\bar{q}$ is velocity vector, $\bar{n}$ control volume surface outgoing nor-

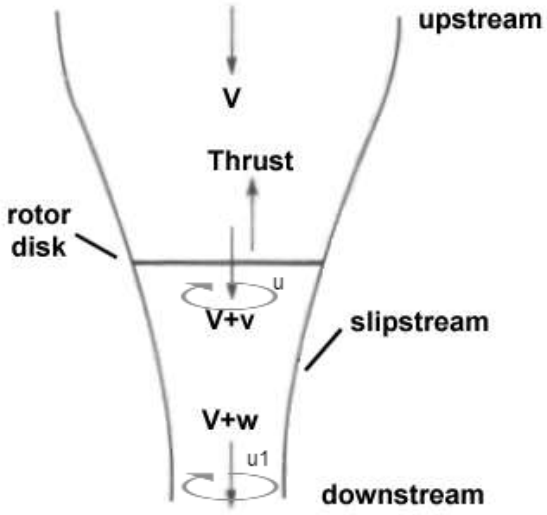

Figure 3.3: Extended momentum theory actuator disk scheme

mal vector, $\bar{F}$ forces resultant and $\bar{M}$ resulting momentum on body.
Fundamental equations are

- Mass conservation law
$$\rho \int \bar{q} \cdot \bar{n} dS = 0 \tag{3.16}$$
- Balance of momenta
$$\bar{F} = \rho \int \bar{q}(\bar{q} \cdot \bar{n}) dS + \int \bar{n} dS \tag{3.17}$$

$$T = \int_{A_d} \Delta p \cdot dA = \int_{S_1} \rho\omega^2 dS_1 + \int_{S_1} (p_1 - p_0) dS_1 \tag{3.18}$$

- Energy conservation law

$$P_i = \int_{A_d} \Delta p \cdot v dA + \int p_{A_d} \frac{1}{2} \rho u^2 v dA \tag{3.19}$$

Expression (3.19) for inducted power, power given by the rotor to flow, appears two different terms: the first one is linked to energy needed to accelerate flow in axial direction and generate thrust. The second term is about energy required to put flow in rotation, in thrust reference this is a loss.
Minimum inducted power condition search is conducted using Euler-Lagrange equation like [2] and is possible to obtain two approximate equations for optimum condition

$$u(r) = \Omega_r \cdot \frac{2v_0^2}{(\Omega_r)^2 + v_0^2} \tag{3.20}$$

$$v(r) = v_0 \cdot \frac{(\Omega_r)^2}{(\Omega_r)^2 + v_0^2} \tag{3.21}$$

Looking at angular velocity variation from 0 to ω through disk, this can be only consequence of torque dQ so is given by

$$dQ = \omega r^2 d\dot{m} = 4\pi r^3 \rho V_\infty (1 + a)\Omega a' dr \tag{3.22}$$

Here appears rotational interference factor

$$a' = \frac{\omega}{2\Omega} \tag{3.23}$$

linked to the kinetic energy loss for flow particles rotation, in this theory viscous energy losses are still not considered.

Chapter 4

Volume finite method

4.1 Computational fluid dynamics

Computational Fluid Dynamics (CFD) is one of the most useful simulation tool nowadays, used as technology enabler. Born to be used in aeronautics and aerospace industry, because of it's flexibility now is an essential tool for a wide range of design industries such as chemical, nuclear, automotive and much more,
Even electronics industry employs CFD to optimize heat transfer and energy systems inside electronic devices, in building industry CFD is used for HVAC in fire simulation and air quality assessment (heating, ventilating and air conditioning). Beside Computational Fluid Dynamics there are other Computer Aided Engineering tools quite used, such as Finite Element Analysis for solid mechanics and vibration, but unlike FEA that is fairly simple to implement on computer, CFD had a delay to become mainstream, this is because the complexity of equations. These are Navier Stokes equations that carry accurately a whole set of flow phenomena from laminar or turbulent single phase incompressible flows, to compressible flows and all type of multiphase flows.
Looking to a fluid simulation scope, the CFD analysis is a practical starting

substitute of wind tunnel. Treat the wind tunnel as a analogical analogical Fluid Dynamic analysis, is easy to see the benefits of using CFD due the second one is cheaper and less cumbersome in term of space. Nowadays the companies who needs to carry a lot of Fluid dynamics simulation, instead rent a wind tunnel for a short period, where they can accomplish only few analysis, they prefer to proceed through a CFD campaign of tests and finally when they are confident enough about the results there are a few tests with wind tunnel. CFD is about studying a real phenomena through simplification of equations and space discretization, this method can be decompose into five steps:

1. Domain modeling.
2. Physical modeling.
3. Domain discretization.
4. Equations discretization.
5. Solution method.

4.1.1 Geometric and Physical Modeling

A physical phenomena usually cannot be understood unless it can be mathematically formulated and then this formulation must be tested and validated. The modeling process contemplate to ignore or simplify a lot of details like transform a three dimensional domain into a two dimensional or a physical component may be replaced by an appropriate mathematical representation. For example a propeller lift can be modeled using a axial symmetric domain to decrease the size of the study domain and then using theory can be written a system of linear or non linear equations to describe the physical results of propeller rotation .

4.1.2 Domain Discretization

The geometric discretization of physical domain leads to mesh on which the conservation equations are eventually solved. Mesh generation requires the subdivision of entire domain into discrete non overlapping cells, these meshes are classified using different characteristics such as orthogonality, cell shape, structure, etc.

To be used with discrete equations are needed topology information, these together with some derived geometric information. Usually these info can be deduce by basic mesh data as element centroid and volume, area, normal direction, etc. Partial differential equations are integrated into each mesh elements produce a set of algebraic equations each one linked to its neighbors. These algebraic equations are then assembled into global vectors and matrices. The integration of the equations for each element is referred as local assembly although the construction of the overall system of equations is referred as global assembly.

Element connectivity

This property relates the local assembly matrix to the global matrix so the equations formed are consistent from one element to another inside computational domain.

4.1.3 Equation Discretization

This step is about transforming partial differential equations into a set of algebraic equations and then assembling into a global matrix and vectors referred as the form

$$A[T] = b \tag{4.1}$$

where T is defined at each interior element and at the boundary of computational domain.

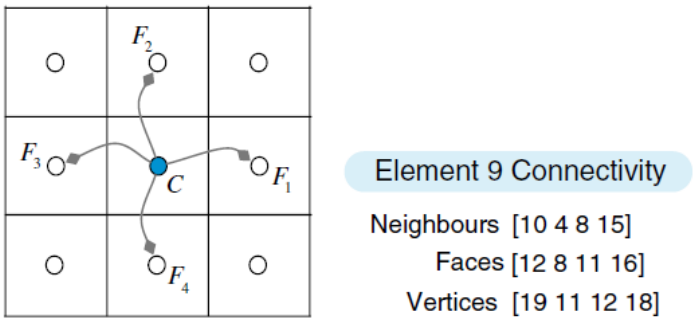

Figure 4.1: Element Connectivity [4]

The equation discretization step is performed for each element of the computational domain to achieve an algebraic relation that link the value of a variable in an element to the values of the variable in the neighboring elements. For the finite volume method the discretization of the equation is obtained by first integrating the differential equation over a control volume or a cell, to achieve a semi discretized form, then approximating the variation of the dependent variable between grid elements to reach the final discretized form.
Increasing the number of grid element leads the solution of the discretized equations approach to the exact solution of corresponding differential equation. This happen because the grid elements get closer together

4.1.4 Solution of the Discretized Equations

To obtain the discrete values of T there must be solved a set of discrete algebraic equations deriving by the discretization of the differential equation. The techniques to solve these algebraic equations are independent of the discretization method, nevertheless unless the algebraic set of equations is linear the solution obtained can be different by one method to another one. Usually the methods can be divided in two types:

- **Direct Methods** The solution of the system of equations is obtained

using a relatively complex algorithm, only once and obtain the solution for a given set of coefficients. Usually, direct methods are not largely used in computational fluid dynamics because of their large computational and storage requirements. In nowadays CFD problems are involved hundred of thousands of cells with a lot of unknowns per cell, moreover A matrix is usually non linear so direct method need an iterative loop to update nonlinearities in A.

- **Iterative Methods** These methods gradually refine the estimated solution by repeatedly solving the discrete system of equations. Iterative methods are particularly suitable for non linear problems and can be implemented with very little storage.

4.2 Volume Finite Method

The Finite Volume Method in Computational Fluid Dynamics is very used because of the high flexibility offered as a discretization method. That was preceded by finite difference and finite element methods, but FVM obtain a prominent role in the simulation of fluid flow problems and related transport phenomena during the 70'.
Lot of the flexibility and popularity of FVM stems from the fact that discretization is managed directly in physical space without need of transformation between physical and computational coordinate system.

4.2.1 Semi Discretized Equation

The finite volume discretization starts with the integration over the elements of the governing equations. The domain is subdivided and then Gauss theorem is applied to transform the volume integrals of diffusion and convention terms into surface integrals.

An example of general conservation equation with a general scalar variable ϕ can be shown as

$$\underbrace{\frac{\partial(\rho\phi)}{\partial t}}_{transient\ term} + \underbrace{\nabla\cdot(\rho\mathbf{v}\phi)}_{convective\ term} = \underbrace{\nabla\cdot(\Gamma^{\phi}\nabla\phi)}_{diffusion\ term} + \underbrace{Q^{\phi}}_{source\ term} \tag{4.2}$$

Steady state form is obtained by dropping the transient term

$$\nabla\cdot(\rho\mathbf{v}\phi) = \nabla\cdot(\Gamma^{\phi}\nabla\phi) + Q^{\phi} \tag{4.3}$$

By integrating over the element **C** shown in the figure 4.2 the equation became

$$\int_{V_C}\nabla\cdot(\rho\mathbf{v}\phi)dV = \int_{V_C}\nabla\cdot(\Gamma^{\phi}\nabla\phi)dV + \int_{V_C}Q^{\phi}dV \tag{4.4}$$

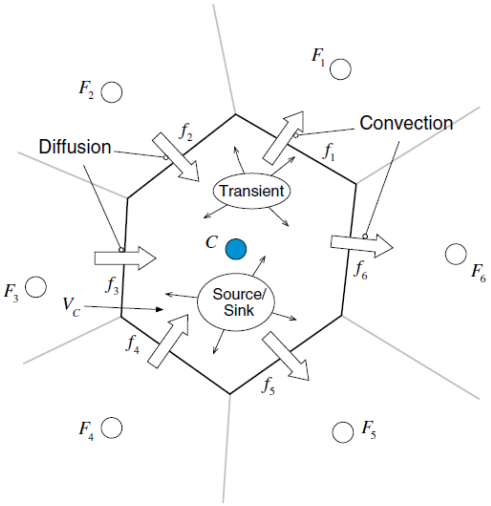

Figure 4.2: Conservation in a discrete element [4]

Then the volume integrals of diffusion and convection terms were replaced by surface integrals through the use of divergence theorem

$$\oint_{\partial V_C}(\rho\mathbf{v}\phi)\cdot dS = \oint_{\partial V_C}(\Gamma^{\phi}\nabla\phi)\cdot dS + \int_{V_C}Q^{\phi}dV \tag{4.5}$$

where Q^{ϕ} represents the source term, S the surface vector, ϕ the conserved quantity and $\mathbf{v}$ the velocity vector.

For a good compromise between accuracy and flexibility while keeping the method simple and relatively of low computational cost is used a one integration point, yielding second order accuracy. The semi discrete steady state equation for element **C** shown in 4.3 can be simplified to

$$\sum(\rho \mathbf{v}\phi - \Gamma^{\phi}\nabla\phi)_f \cdot S_f = Q_C^{\phi} V_C \tag{4.6}$$

Using a flux linearization the (4.6) can be transformed into an algebraic equation by expressing face and volume fluxes in terms of values of variable at the neighboring cell centers.

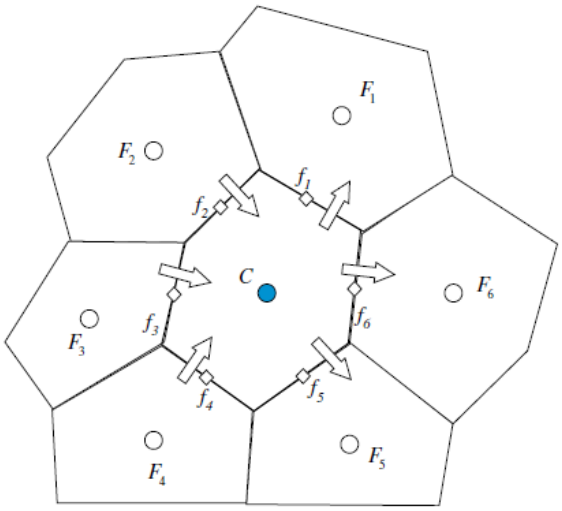

Figure 4.3: Fluxes at element surfaces [4]

4.2.2 Boundary Conditions

The evaluation of fluxes at the faces of a domain boundary does not require a profile assumption. Usually is performed a direct substitution. There are a

wide range of type of boundary conditions, but the most widely used are the Dirichlet and the Neumann boundary conditions.

- **Value Specified (Dirichlet BC)**
  This boundary condition assume a scalar value as known and this value is used to evaluate the boundary flux by substitution.

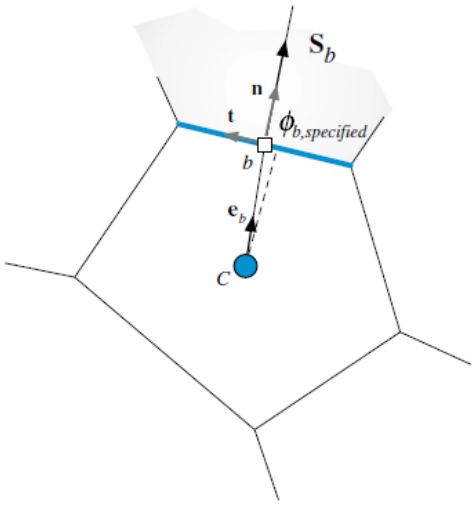

Figure 4.4: Dirichlet boundary condition [4]

- **Flux Specified (Neumann BC)**
  Considering a case where the boundary face of element C represent a physical wall where the ϕ flux quantity is specified. The Neumann condition substitute the flux quantity.

4.2.3 Properties of Discretized Equations

While the size of the element tends to zero, the numerical solution i s expected to tend to the exact solution of the general conservation equation (4.3). However, it is essential for the discretized equations to posses some properties, since finite volumes are used, in order to ensure a meaningful solution field.

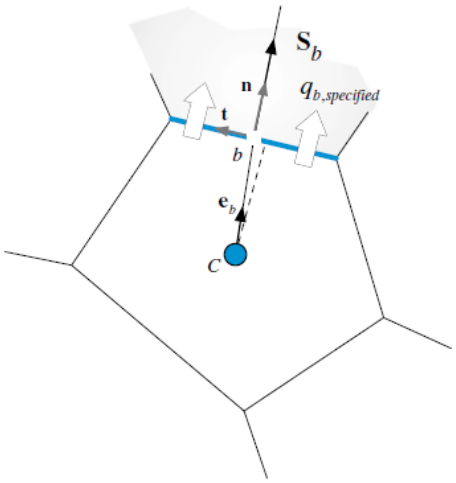

Figure 4.5: Neumann boundary condition [4]

Conservation

Is very important, in a physical point of view, that the transported variables, generally conservative, to be conserved in the discretized solution domain too. For any surface common to two elements, the flux entering the face of one element will be exactly equal to the flux leaving the other element through that same face. Thus these fluxes are of equal magnitude and opposite signs.

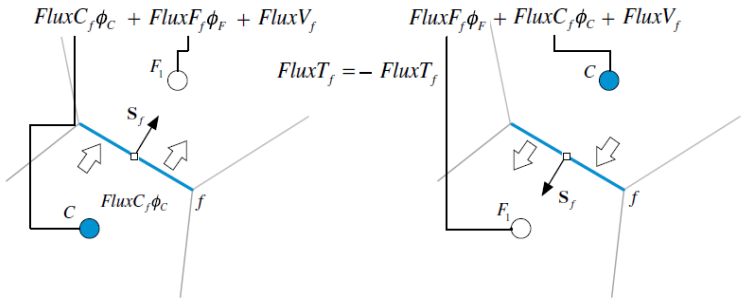

Figure 4.6: Fluxes on neighboring elements [4]

Accuracy

This property refers to how close numerical solution is to exact solution. However, in general the exact solution for the problem to be solved is unknown so the direct comparison to check accuracy is not possible. An alternative is to consider as measure of accuracy the truncation error.
With a first step discretization has an error associated of $O(x - x_f)^2$ represents a second order of accuracy. The discretization error does not returns the value of the error on a certain grid, instead is index of how fast the error will decrease with grid refinement. The higher the order of the error the faster it will decrease increasing mesh refinement.

Convergence

To deal with nonlinear nature of conservation equations is needed an iterative approach. The solutions are obtained by repeatedly applying a solution algorithm with the solution obtained at the end of an iteration stating with an initial guess. A solution is said to be converged when it does not change more as iterations progress. In general, a solution is settled converged when the changes between two consecutive iterations returns a negligible quantity ϵ.

Consistency

A solution to an algebraic equation that approximate a partial differential equation is established as consistent if, at each point of solution domain, the numerical solution approaches the exact solution of partial differential equation as grid spacing and time step tend to zero.

Stability

This property refers to the behavior of discretized equation to be solved by an iterative solver, whether the resulting system of algebraic equations can be

solved under a wide range of initial and boundary conditions.
For transient problems, a stable numerical scheme keeps the error in the solution bounded as time marching proceeds. The use of explicit or implicit transient schemes has direct impact on the stability of the numerical method. The stability of explicit methods is guaranteed by limiting the size of the time step.
On the other hand, the stability of implicit methods can be enhanced by under-relaxing the discretized set of algebraic equations either through the use of under relaxation factors or by applying the false-transient approach [4].

4.3 Finite Volume Mesh

A crucial role in the implementation of the finite volume method is setting up a geometrical support framework. This process begins with mesh generation, or rather the replaces of continuous domain by a discrete one formed of a contiguous set of non overlapping elements, delimited by a set of faces and setting some of these faces as boundary faces. After this there is the computation of relevant geometric information of various components of computational mesh and at last is completed by capturing the topology of these components.
So the finite volume mesh is the combination of the domain discretization with his geometric properties and the topological information about their arrangement and relations.

4.3.1 Domain Discretization

The discretization of physical domain, as said as mesh generation, produces a computational mesh 4.7 on which the governing equations are solved.

In general a geometrical domain can be discretized using either a structured or an unstructured grid system. A structured grid system has many coding and performance advantages but suffers from a limited geometric flexibility,

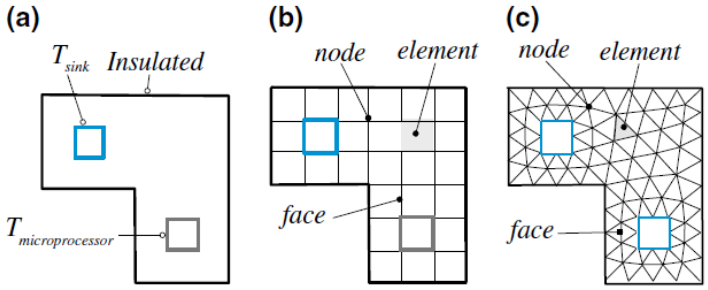

Figure 4.7: **a** Domain of interest, **b** domain discretized using a uniform grid system, and **c** domain discretized using an unstructured grid system with triangular elements [4]

more flexibility can be achieved using multiple blocks to define the geometry 4.8.

To make the mesh generation more flexible it could adopt an unstructured mesh with explicit topological information based on geometric entity numbering and connectivity tables 4.9.

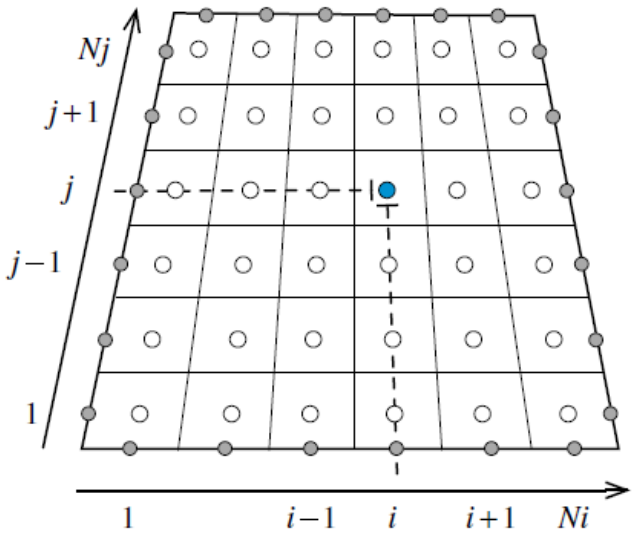

Figure 4.8: Structured mesh index and topology [4]

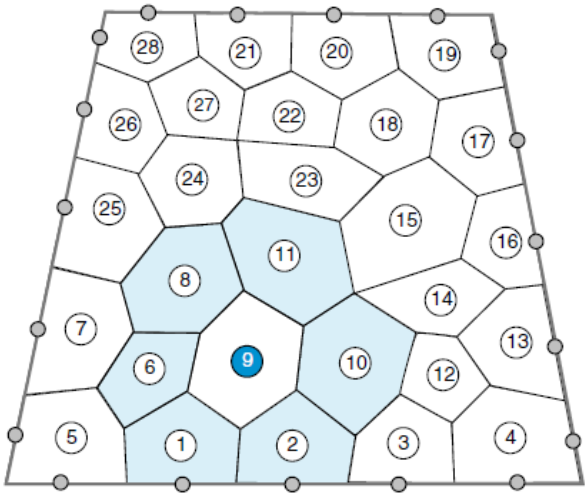

Figure 4.9: Unstructured mesh index and topology [4]

4.3.2 Mesh type

Focusing on mesh type there are basically two major typologies used for discretize the geometrical domain, assuming a three dimensional field can be seen

- **Trim**

  This type of mesh is a structured mesh formed by cubic cells with defined dimension, cut in the proximity of domain border. Trim mesh is aligned along the global reference system and the height and length of each cell layer is defined by user's parameters. Usually this mesh is used for problems where the fluid to study is nearly uni dimensional and aligned with the body geometry, like a wind tunnel car simulation.

- **Polyhedral**

  This type includes a wide range of mesh depending on the number of faces of the cells, increase this parameter return a better simulation, on the other hand this will increase the computational cost. Polyhedral mesh usually is used for simulations where the direction of flow post

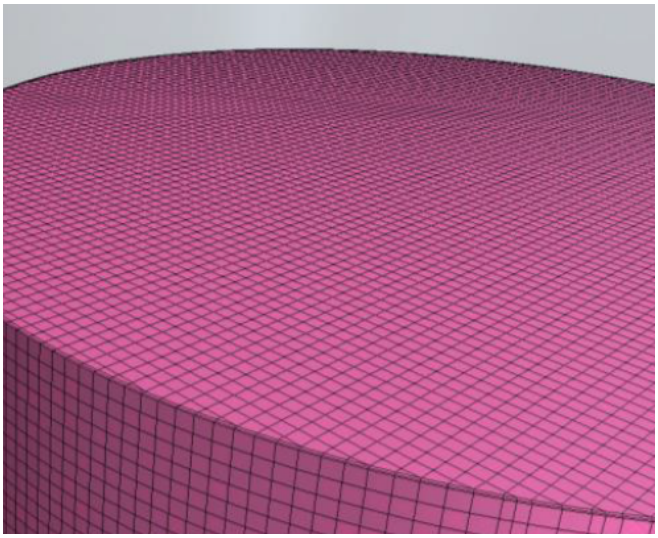

Figure 4.10: Trim mesh

interacting with the body is unknown.

4.3.3 Overset Mesh

Overset meshes, also known as "Chimera" or overlapping meshes, are used to discretize a computational domain with several different meshes that overlap each other in an arbitrary manner. They are most useful in problems dealing with multiple or moving bodies, as well as optimization studies [5]. Using Overset mesh, the computational domain is covered by a number of grids which overlap with each other in an arbitrary manner. An advantage of such grid arrangement is the possible employment of grids of high quality (e.g.cylindrical, orthogonal, spherical grids) when handling complex geometries. The grid components can be altered to represent the nearly shape of real-life geometries, thus returns a great deal of flexibility for multi connected domains discretizations.

The overlapping grid techniques, differently from unstructured mesh, offer much more flexibility where are problems that involve multiple bodies in rela-

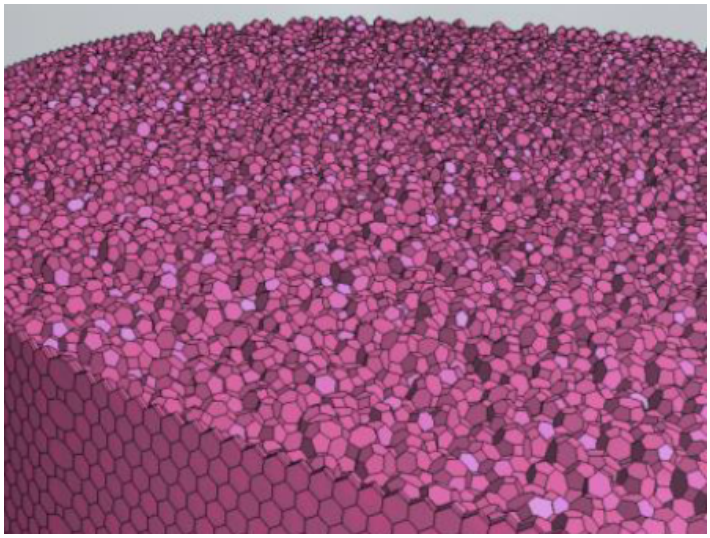

Figure 4.11: Polyhedral mesh

tive motion. In that case, as the component grids move relative to each other, only the location of boundary points at overlapping interfaces that are involved in interpolation changes. The grid points do not need to be regenerated and the grids retain their topology and geometrical properties. Furthermore, in the optimization studies one needs often to modify the geometry (e.g. to exchange one part of a configuration with a new one) while searching for the optimal design.

As a consequence, in most cases a new grid has to be generated for the new configuration. Overlapping grid techniques offer also in this case a great flexibility, since the grid, if at all, usually needs to be modified only locally (e.g. around a new part).

The use of unstructured overlapping grids permit to reduce the computational domain that in return reduces the complexity of the overlapping grid systems.

Overlapping grid methodology

The basic elements of the overlapping grid technique are

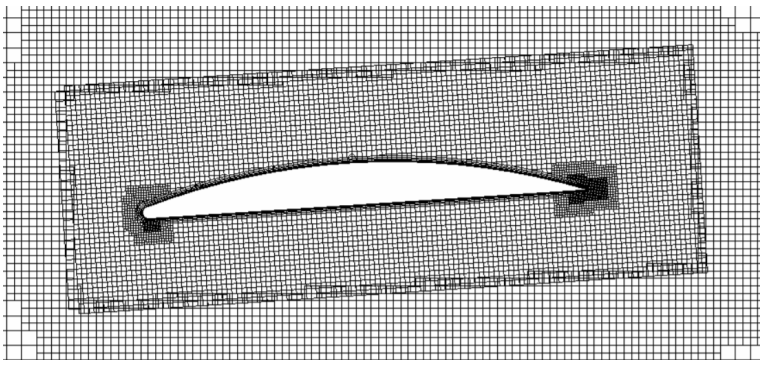

Figure 4.12: Overset mesh example

- decomposition of computational domain into sub domains, then generation of a suitable grid for each sub domain.
- development of a coupling method to obtain an efficient, accurate and unique solution of the governing equations for the overlapping grids.

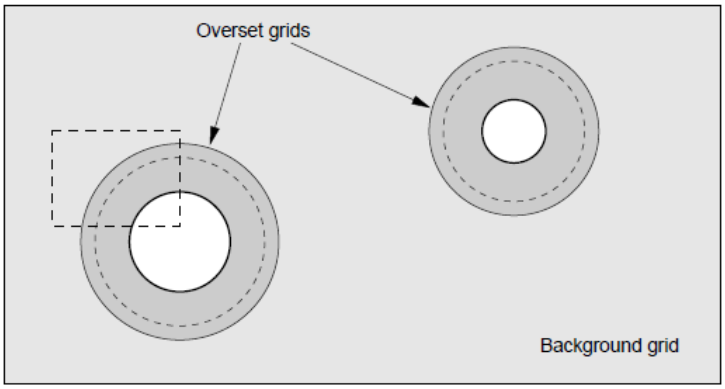

Figure 4.13: An overlapping grid system consisting of two minor grids attached to the bodies and embedded into major background grid stretched over the entire domain [5]

As shown in figure 4.13 there are two separate grids around each body, the remaining part of the domain is covered by another grid also called *Background*

grid. In the case of moving bodies it might be necessary to keep all grid cells, since, due to body motion, different parts of the grid are covered by the bodies at different times.

Therefore, the cells which are covered by the bodies are deactivated rather then removed. These cells are called inactive cells. In order to separate inactive cells from the rest of the domain, an artificial boundary within the background grid has to be created. Nodes in the centers of cells along such a boundary within a background grid are denoted with "$\circ$" in figure 4.14, which shows a detail of the overlapping region masked by the dashed rectangle in figure 4.13. The variable values at these cells and cells along the outer boundary of the overset body grid (denoted with "$\bullet$") are obtained by interpolation of the variable values from the other component grid (donor grid).

According to their role in the solution process of the governing equations, the cells in an overlapping grid system may be divided into three groups: discretization (active), interpolation, and inactive (hole) cells. Discretization cells are used to discretize governing equations, interpolation cells receive the solution information by interpolation and inactive cells are disregarded during the solution process. All three cell types are shown in figure 4.14.

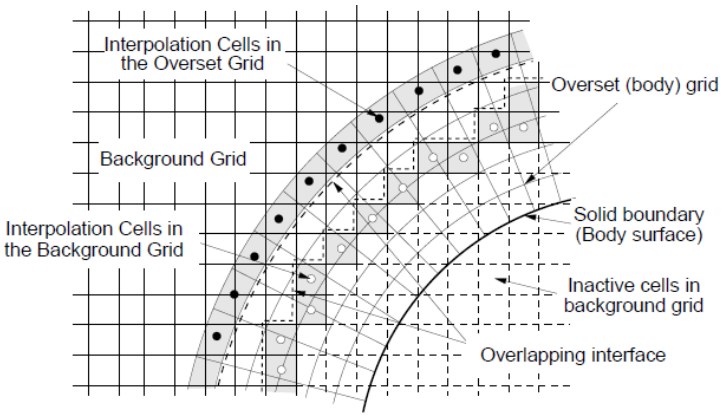

Figure 4.14: A detailed view of the overlap region with some definitions and notation [5]

A special implicit procedure for coupling of the solution on overlapping grids is developed. The interpolation equations used to compute the variable values at interpolation cells distributed along grid interfaces are involved in the global system of linearized equations that arise from discretization. Such a modified linear equation system is solved for the whole domain providing that the solution is obtained on all grids simultaneously.
In this way a strong inter grid coupling characterized by smooth and unique solution in the whole overlapping region and a good convergence rate is achieved. The mass conservation, which is violated by interpolation, is enforced by adjusting the interface mass fluxes.

Chapter 5

Propeller analysis

Next step of the thesis is to simulate and analyze a propeller whose thrust and torque characteristics are known. To analyze this problem, first thing to do was to go on a CAD software and design a parametric propeller so a simple $12''$ diameter propeller was made using *DDS Catia* CAD software. After that is important to defining some operating points and the environment where the propeller has to work, to do this the company allowed me to meet the client who financed this project, after a talk were chosen the reports to observe and the operating points, will be described in the physics section.

5.1 Preliminary works

5.1.1 DDS Catia

As already said, the propeller analysis starts on a CAD software, to be able of launch a optimizer software that works on parameters is crucial to model a parametric propeller. For the design of propeller is been chosen a classical commercial model and have a simple shaft without warhead. The chosen parameters are the next

- Pace

- Shaft Height
- Taper Angle
- Starting Angle

Through a parametric analysis the thesis search for a optimization of the propeller in question. Below are shown some views of the modeled propeller inside *Catia*.

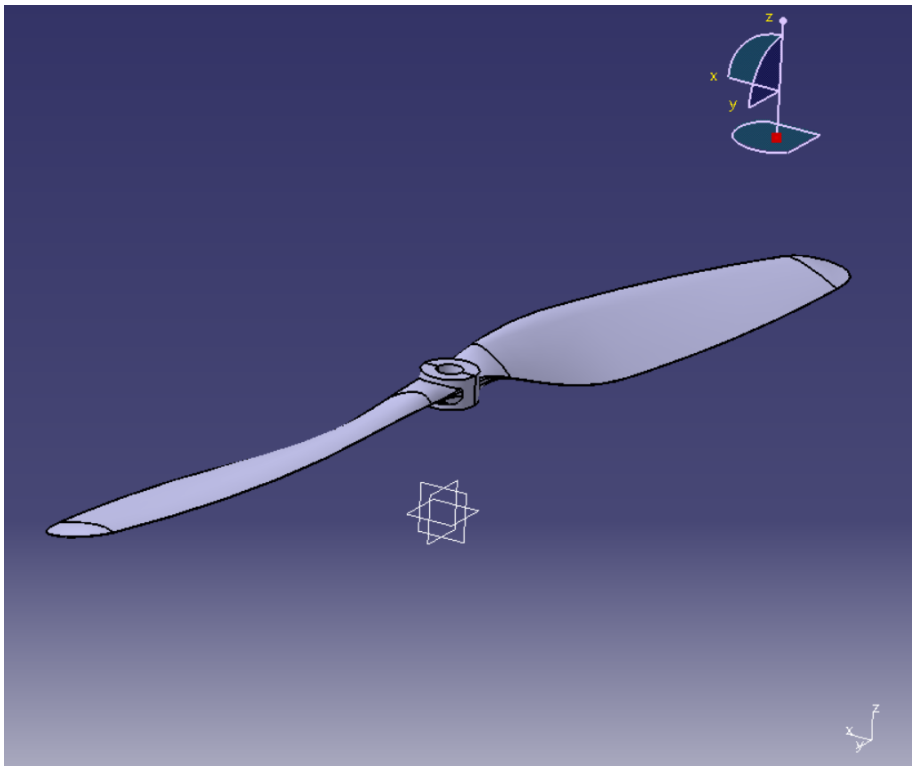

Figure 5.1: Catia isometric view

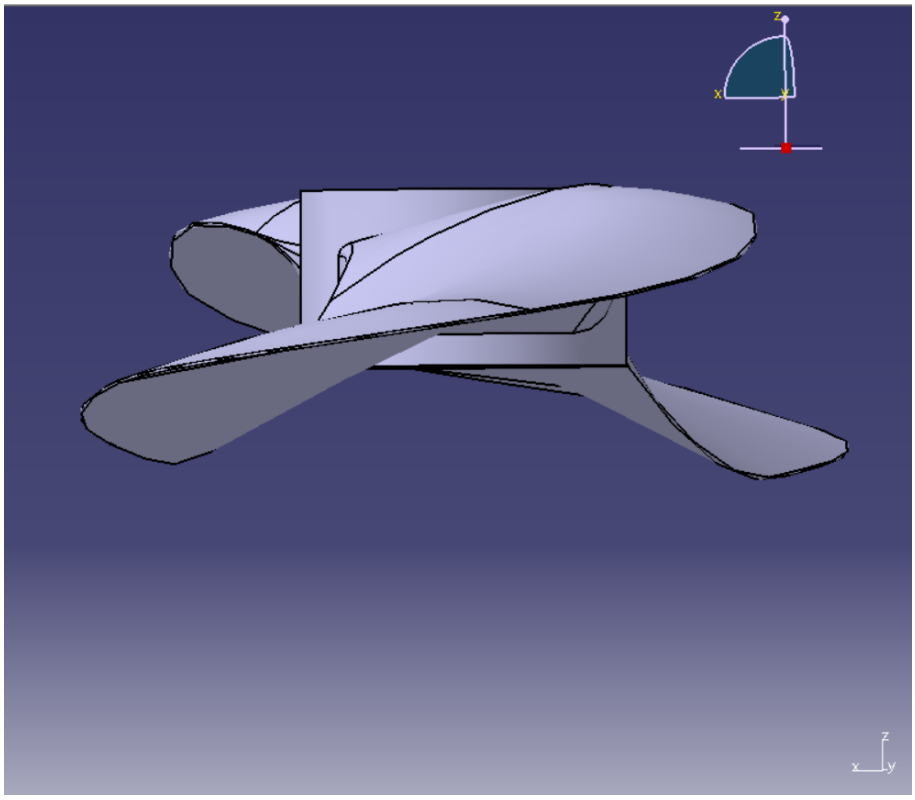

Figure 5.2: Catia Front view

5.1.2 STAR CCM+

To transfer the propeller to the CFD software the model is been exported as an IGS file that is a graphics file saved in a 2D/3D vector format based on the Initial Graphics Exchange Specification (IGES).
Inside *STAR* the propeller need to be repaired because during the exportation the surfaces are a bit modified and some complex patterns were generated, these patterns usually seen some surfaces permeate together and errors are born, without the repair of the surfaces and the delete of these errors the CFD analysis is impossible and leads to mesh problem. This type of work is very methodical and needs an amount of patience to eradicate all the free edges and the pieced edges, but at the end of this the propeller is ready to be putted inside the analysis that now has to be set.

5.2 Operating points and physics

As already said the operating points and the physics were chosen after a speech with the client of the project, this leads to the definition on the physics inside the software, but the data given by the client are not suitable to the software.

5.2.1 Client data

The request of the client is about a parametric optimization of a propeller that is operating at two different project points.

- Max thrust at 3600 rpm.
- Hovering at 2500 rpm

These two status are achieved at an altitude on 300 meters above the sea level, to obtain the data about this altitude is needed to start working on the ICAO standard. Also known as the ICAO Standard Atmosphere, ISA is a standard

against which to compare the actual atmosphere at any point and time. The ISA is based the following values of pressure, density, and temperature at mean sea level each of which decreases with increase in height:

- Pressure of 1013.2 millibar
  Pressure is taken to fall at about 1 millibar per 30 feet in the lower atmosphere (up to about 5,000 feet).

- Temperature of +15 °C
  Temperature falls at a rate of 2 °C per 1,000 feet until the tropopause is reached at 36,000 feet above which the temperature is assumed to be constant at -57 °C. (The precise numbers are 1.98 °C, -56.5 °C and 36,090 feet).

- Density of 1,225 gm/m3.

The real atmosphere differs from ISA in many ways. Sea level pressure varies from day to day, and there are wide extremes of temperature at all levels. To determine the air characteristics are used these data. A k coefficient appears to define the thermal gradient with whom the temperature decrease as the altitude increase $k = 0,0065\ \frac{K}{m}$ and this coefficient is used together with R Air state equation constant and g gravitational constant to create a new constant

$$n = \frac{1}{1 - k\frac{R}{g}} = 1,23496 \tag{5.1}$$

To obtain the characteristics are used the next equations

$$T = T_0 kz \tag{5.2}$$

Considering z as the altitude in question, this is the simplest because use only the thermal gradient. For density distribution the polytropic relation is used

$$\rho = \rho_0 \left(\frac{T}{T_0}\right)^{\frac{1}{n-1}} \tag{5.3}$$

And the pressure is obtain with state equation

$$P = \rho. * R. * T; \tag{5.4}$$

To use this equations are needed the reference value of temperature and density, $T_0 = 288.16\ [K]$ and $\rho_0 = 1.225\ \frac{kg}{m^3}$. So plotting the trend of the normalized air characteristics

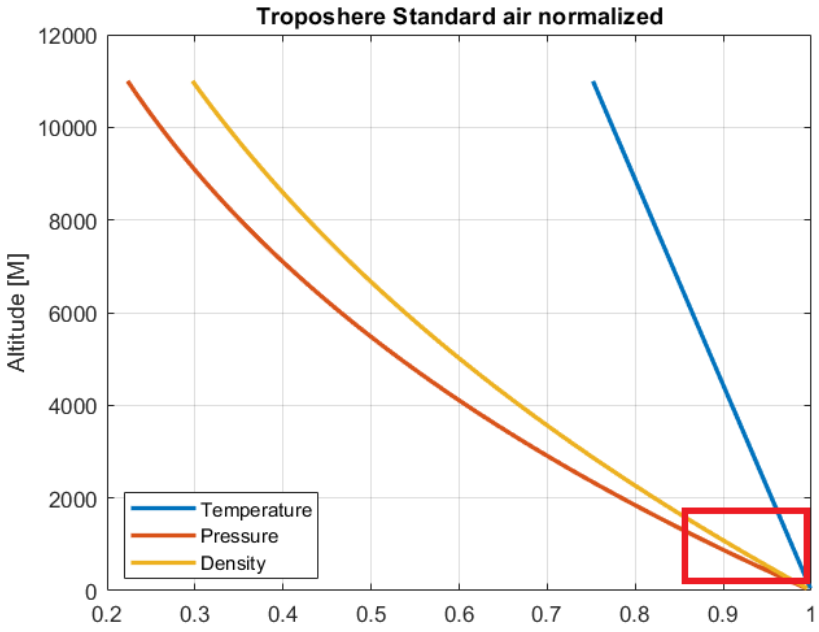

Figure 5.3: Troposphere ISA normalized characteristics

Using the *Matlab* code written the air characteristics at 300 meters above the sea level obtained are

- Temperature: 286.21 $[K]$
- Pressure: 97775 $[Pa]$
- Density: 1.190 $\frac{kg}{m^3}$

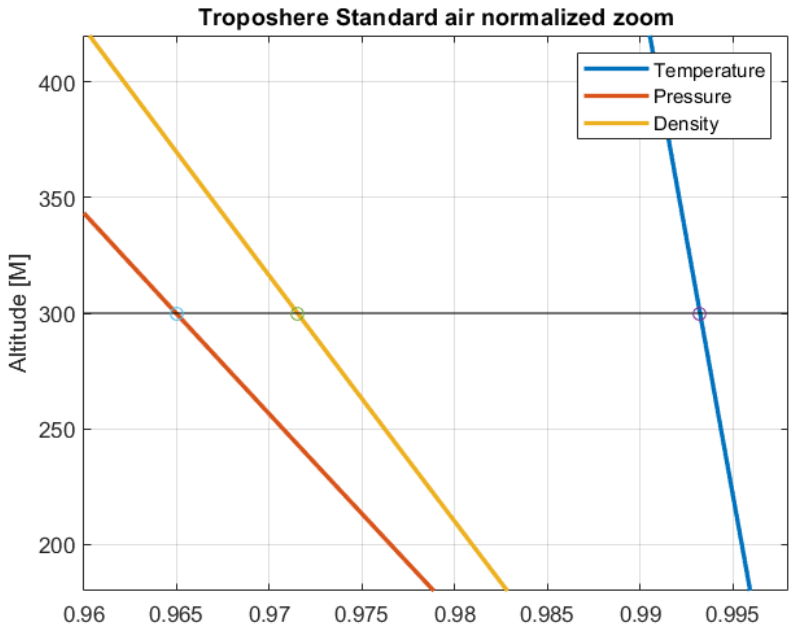

Figure 5.4: Troposphere ISA normalized characteristics zoomed

5.3 Regions and motion

To proceed with the analysis is created the environment inside of which the propeller will be analyzed, this region is a cylinder on 2 meters of radius an 3 meters of height positioned to lay with 1 meter above the propeller and 2 below. To perform a rotation CFD simulation there are 2 methods, the **DFBI** Dynamics Fluid Body Interaction that study a body rotating in the mesh and how it reacts to the flow passing next to it, this type of simulation is quite expensive in terms of computational cost, is suggested for complex analysis where there are several bodies in the same space. Instead for a simpler analysis is better to use a **RFR** Rotating Frame Reference, namely this method is about the creation of a Rotating domain inside the Environment domain so to the first one is applied a rotating frame definition. This method is cheaper in terms of computational cost so is better for an analysis of a simple rotating propeller.

5.3.1 Rotating Domain

Using the Rotating Reference Frame method is crucial to well size the Rotating domain, because a bad sizing of this domain can lead to computational error and so to wrong results. So as a side analysis in this thesis are performed a multiple steady analysis of the propeller using different dimension of rotating domain.

- Cylinder of diameter 1.2 times the propeller's one and 5 times the height of propeller. So the dimensions are 300 mm of diameter and 50 mm of height.
- Cylinder of diameter 1.5 times the propeller's one and 10 times the height of propeller. So the dimensions are 375 mm of diameter and 100 mm of height.

- Cylinder of diameter 2 times the propeller's one and 15 times the height of propeller. So the dimensions are 500 mm of diameter and 150 mm of height.

- Cylinder of diameter 3 times the propeller's one and 20 times the height of propeller. So the dimensions are 750 mm of diameter and 250 mm of height.

Below in 5.5 is shown the fourth case in a geometry scene to let visible the dimensions related to the propeller.

Since is created a rotation domain when the boundary conditions are imposed

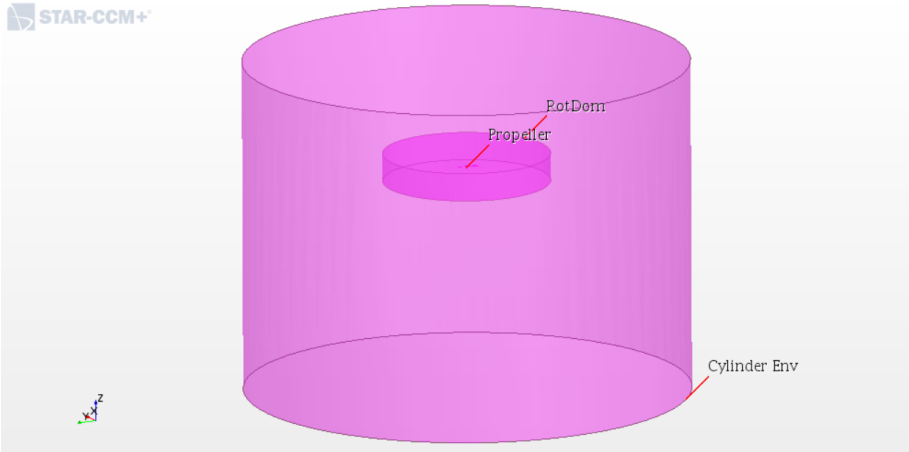

Figure 5.5: Geometry scene of analysis domain in STAR CCM+

is important to remember to create an interface between the Rotating domain surfaces that are present inside both the regions and as long as is used an entire domain and not a symmetry splitted one the interface to use is an internal interface.

5.4 Mesh

To proceed through the simulation is mandatory to achieve a good mesh of the geometry to obtain reliable results and similar to real results obtainable using a real simulation inside a wind tunnel.
To create a new mesh the software offers two possibilities, using an *Automated Mesher*, this one grants a limited freedom during the mesh generation, but is optimized for the new users thanks to the linear and clear workflow to follow. The other one mesh generation type is through a *Continua mesh*, for an advanced user allow to finer tuning of the mesh parameters. Inside this elaborate is used the second one to take advantage of the widest freedom inside the customization of the mesh.
The mesh chosen is a polyhedral with prism layer, and the relative settings are base size of 1 meter, this choice is only for the environment cylinder where the course of the air flow is not of primary importance, as we approach to the propeller the mesh will became finer using some refinement with smaller cell size. Another setting modified is growth factor reduced to a 0.6, this one describe a smoother gradient to shift from a mesh to another, crucial for create a good mesh without strong differences between meshes.

5.4.1 Prism layer sizing

The most important setting of a viscid simulation is the prism layer setting, without this the simulation cannot capture the viscous sublayer and the results are not reliable, so is indispensable to design a good prism layer mesh to achieve an accurate simulation results.
The prism layer settings requested by the software are thickness and number of layers, the first one is strongly bounded to the Wall treatment that is choose to follow for the analysis, besides the number of layers grants a greater accuracy

for the acquisition of the velocity of the boundary layer.

To evaluate the prism layer thickness is used the Reynolds formula.

$$Re_x \approx \frac{\rho(\Omega 0.75R)C_{0.75R}}{\mu} = 37920 \tag{5.5}$$

In the 5.5 is used a density of 1.19 $\frac{kg}{m^3}$ and dynamic viscosity of $1.85 \cdot 10^{-5}$ Pas, finally the $C_{0.75R}$ is the chord measured at 75% of radius equal to 23.77 mm. To obtain the thickness is used the inverted Reynolds formula using a U_∞ that is the tangential velocity at the 75% of radius that is equal to 24.5 $\frac{m}{s}$.

$$\delta = \frac{\mu}{\rho U_\infty} Re_\delta = \frac{\mu}{\rho U_\infty} (\frac{6}{50} Re_x)^{\frac{6}{7}} = 0.8mm \tag{5.6}$$

The results of this calculation return a value of 0.8 mm so to be safe the prism layer thickness is overestimate to 1 mm 5.6 assuming that this chosen value grants to cover the entire boundary layer, later this assumption will be verified as plausible or not.

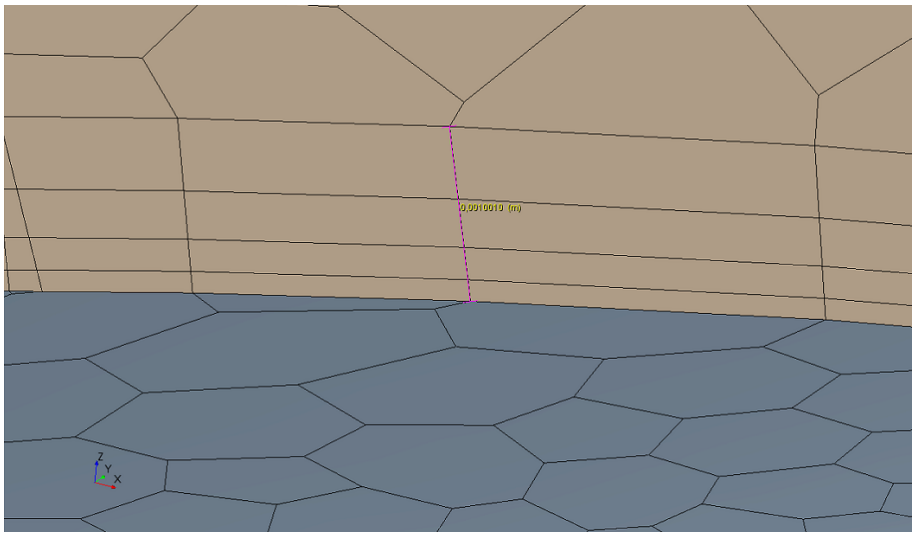

Figure 5.6: Prism layer obtained

After a simulation the velocity inside the prism layer was inspected and using

as reference plane the 0.7% of propeller radius was reported that the first sizing of the prism layer using a 1 mm of thickness was overestimated. As is possible to see in the 5.7 the active cells where is capture the velocity gradient are too few, and the extension of the prism layer is exaggerated so it was chose to halve the thickness of the prism layer obtaining 0.5 mm of thickness.

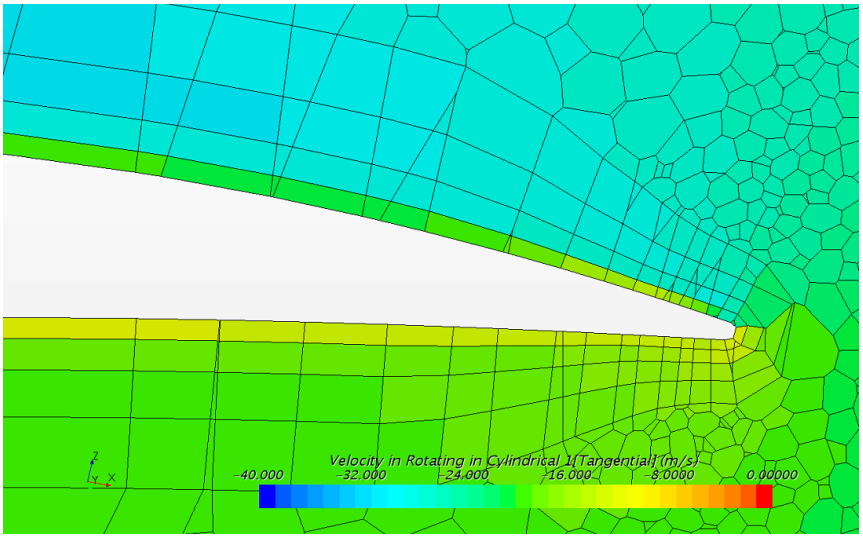

Figure 5.7: Look at prism layer thickness and effective capturing

For the comparative and the simulations was chose to perform for each rotational domain a set of four different number of prism layer solutions. So the sets used are $[4, 8, 12, 16]$, the results will be described afterwards.

5.4.2 Refinement

To obtain a good mesh, maintaining a low number of cells, is essential to create a great number of volume refinements that are used to refine the mesh and decrease the cells dimension according to the geometry and the necessity that are request for simulation.
As the first account the simulation was provided of 5 different layers of refinement, listed below

- Rotary refinement
  This one is quite important because it appears to be intimate entangled to simulation's results. It emerged that if the cell's size is not at least 5 times minor of the rotary domain diameter the results will not converge. Figure (5.8).

- Wake refinement
  Used to capture the wake below the propeller, is a simple cylinder with 300 mm of diameter and 850 mm of height starting at 30 mm below the propeller. Figure (5.8).

- Inner refinement
  A capsule around the propeller to create a first layer of refinement for the surface's propeller, long 400 mm and wide 200 mm. 5.9

- Shaft refinement
  This one is a combination of two cylinder to encapsulate the shaft curvature. Figures (5.10 and 5.11).

- General edge refinement
  To improve the edge without wasting cells the forced choice was to add another set of refinements on the edges of propeller. For the first simulation it was chosen to use the Star CCM+ cylinder creation.
  Were created and manually positioned 14 cylinder with 2 mm of diameter all around the propeller. Figures (5.12 and 5.13)

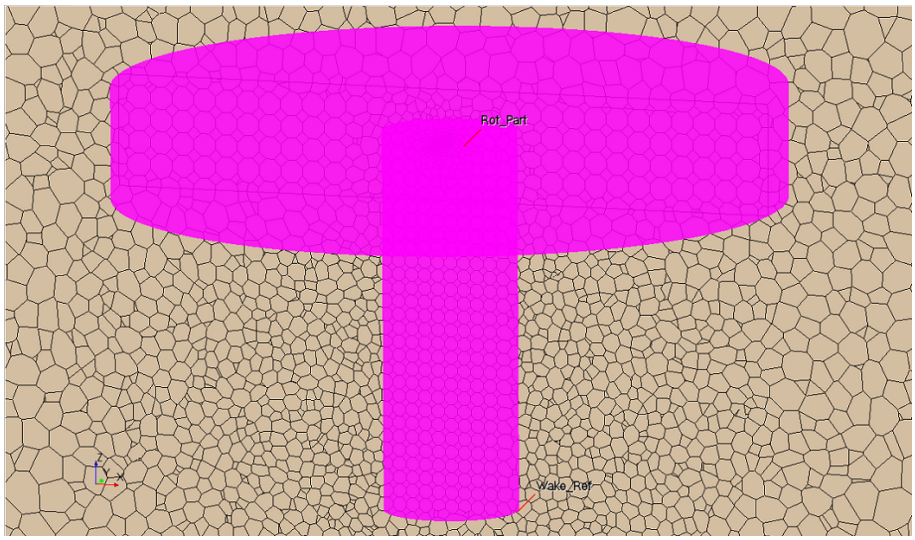

Figure 5.8: View of Rotary and Wake Refinement

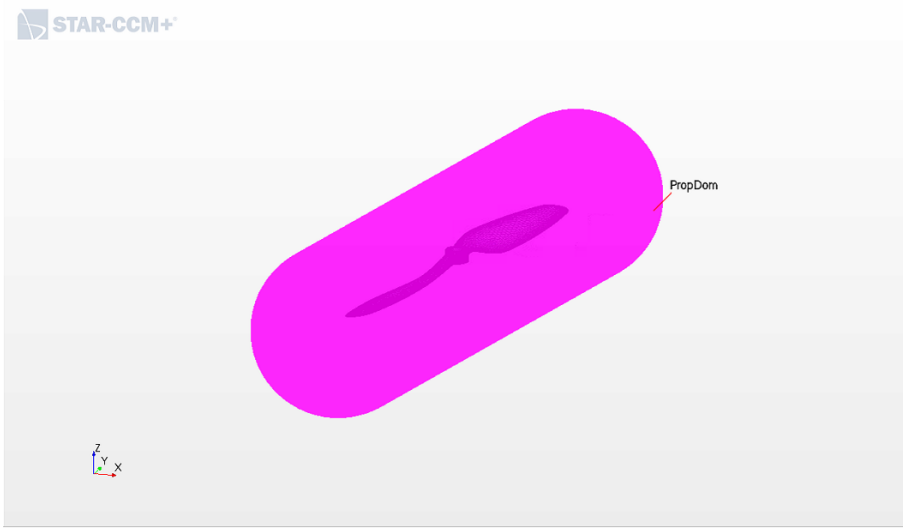

Figure 5.9: View of Inner refinement

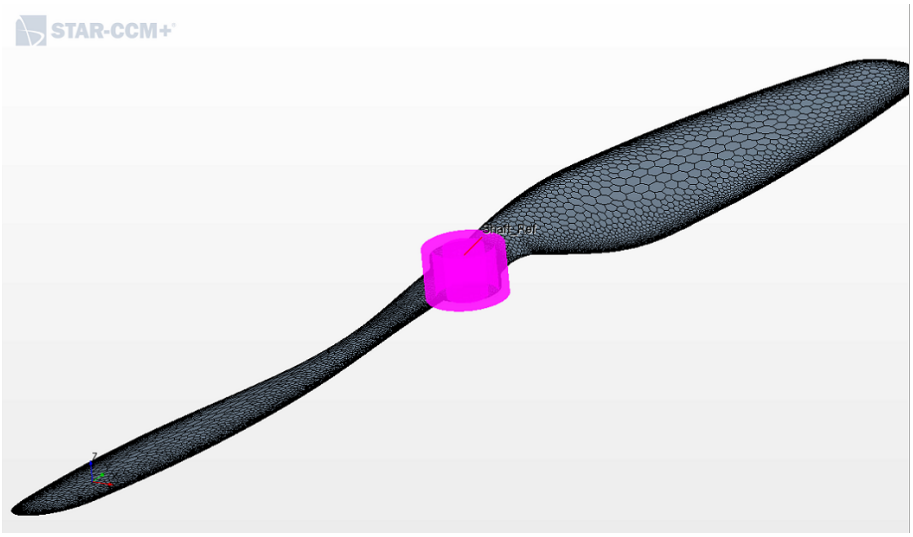

Figure 5.10: Isometric view of shaft refinement

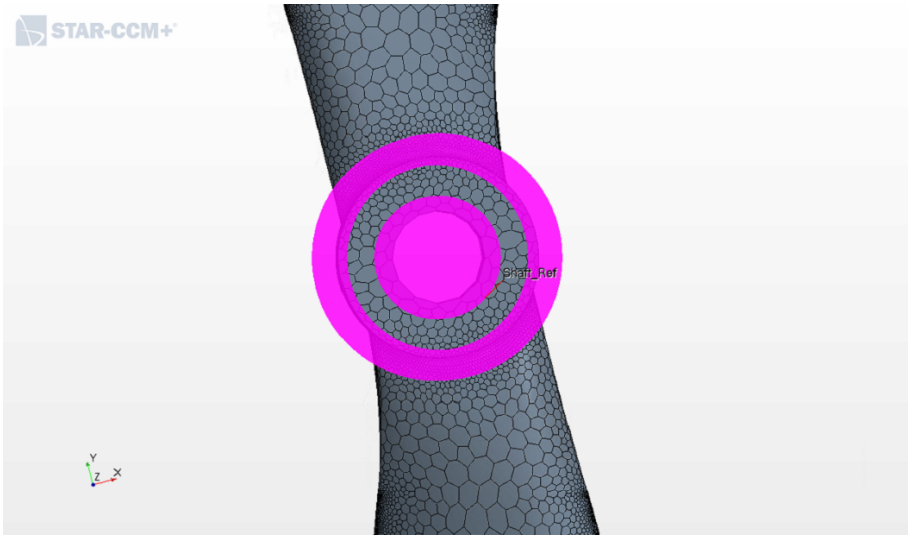

Figure 5.11: A top view of the shaft refinement

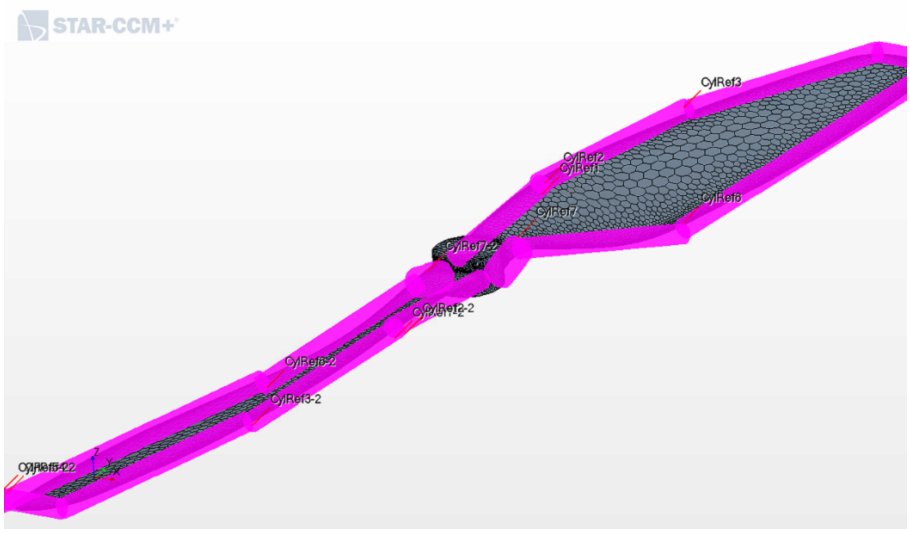

Figure 5.12: Isometric view of general edge refinement

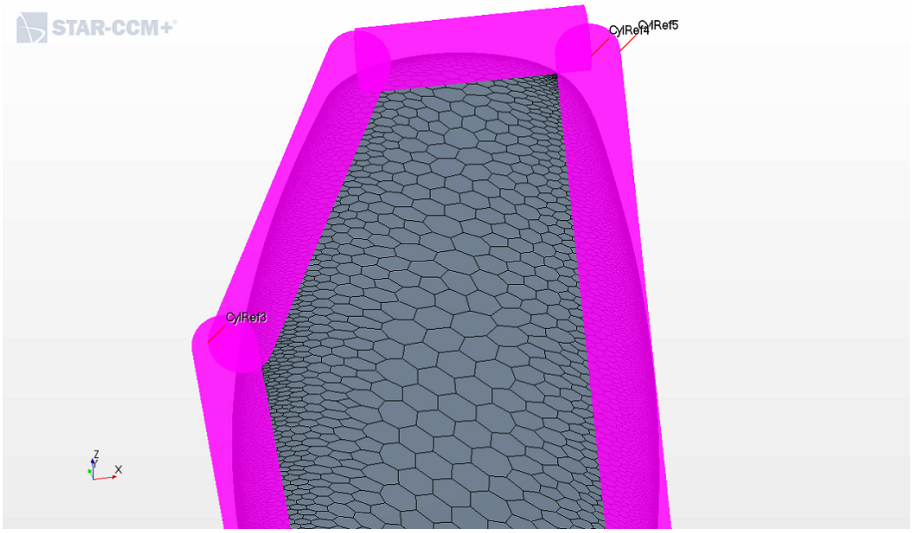

Figure 5.13: Top view of general edge refinement

A first set of simulations was performed using only these refinements, this set is called "*Low Edge Def*", in the next section will be better described to ensure to understand the mesh dimensions treated.

The second set of simulations were implemented adding a new bunch of refinement, this was done to improve the results without waste of cells due of a not well designed cylinders around the edges. So to increase the number of cells, but only where are really necessary it were created a new series of edge and shaft refinements, to achieve this goal it was unavoidable to turn back to the CAD software (5.14).
So taking the CAD it was created a circular sweep around the edge of propeller, to have more flexibility this new refinement was splitted into three parts. Moreover a finer shaft refinement was made always to reduce the number of cells where are not necessary.

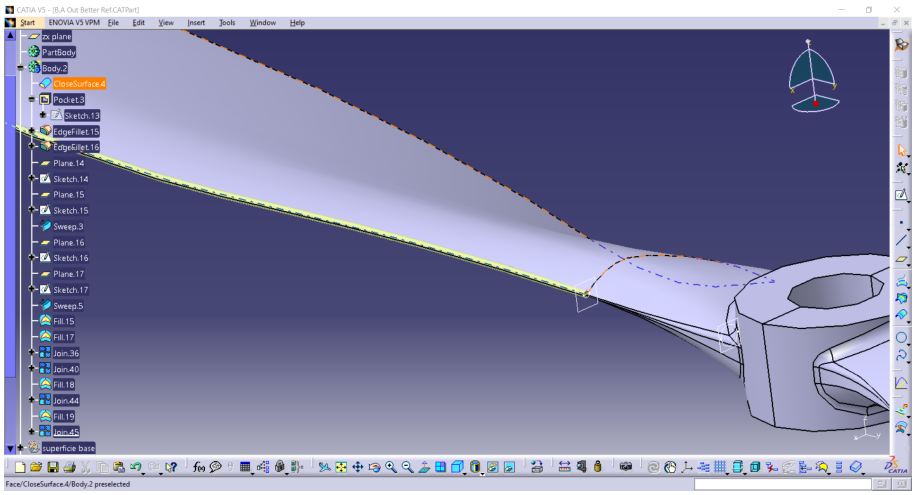

Figure 5.14: A view of the refinement in *Catia*

For this second set of simulations the refinement used were the previous set to which the following are been added

- Edge refinement
  This as already said was splitted into Leading, Tip and Trailing to have wider chance and plasticity to tuning the mesh values. The entire set is a cylinder swept on the edge with a diameter of 0.5 mm.Figures (5.15 and 5.16).

- Shaft refinement
  This refinement is a set of cylinders rested on the shaft blend with a diameter of 0.5 mm. Figures (5.17 and 5.18)

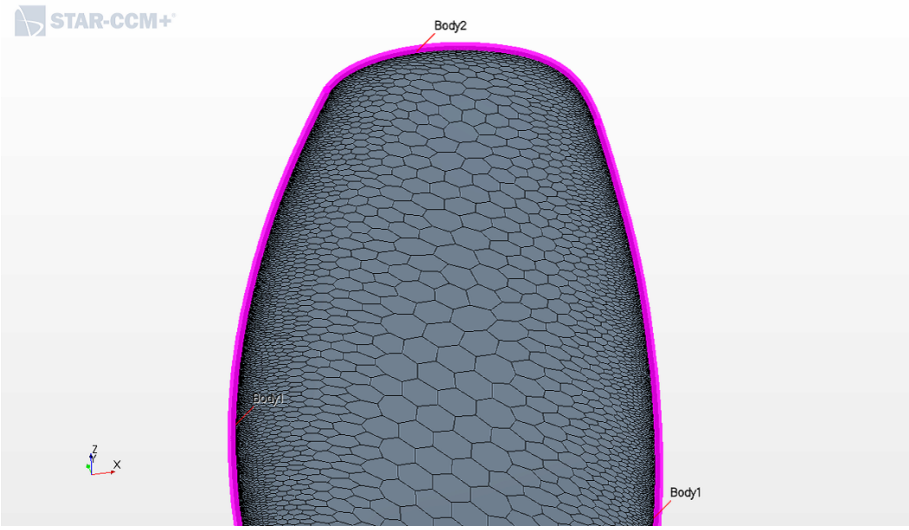

Figure 5.15: Top view of edge refinement

This set of refinement is called "*Edge Ref*" to distinguish from the previous and the next set that are always of edge, but using a different dimension of the cylinders of refinement.

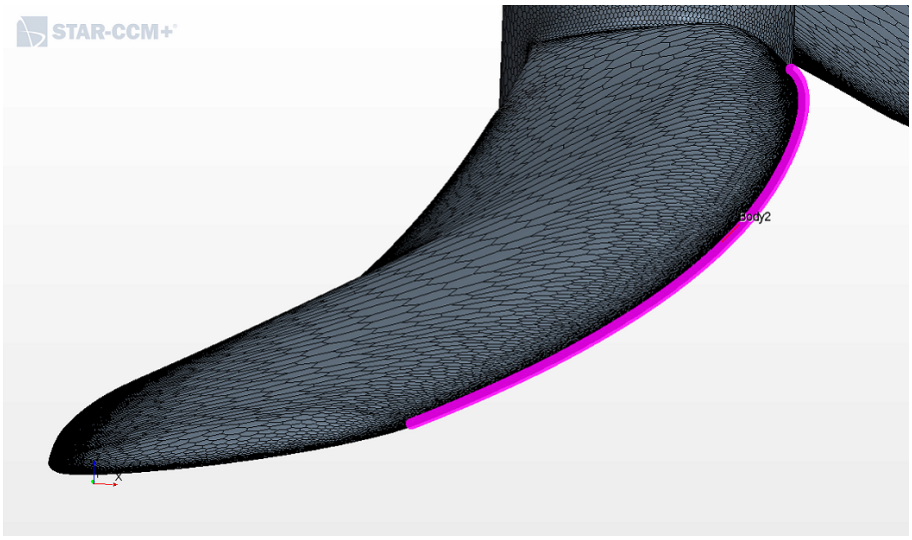

Figure 5.16: Isometric view of edge refinement

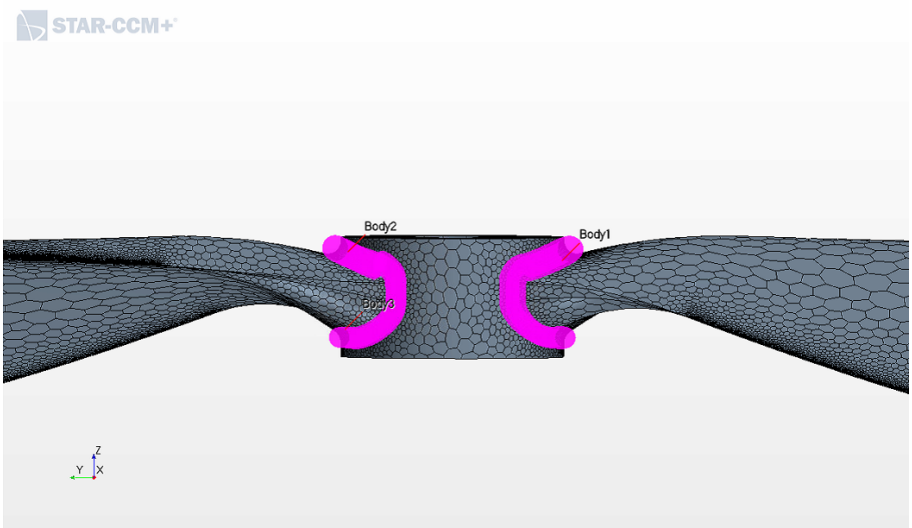

Figure 5.17: Lateral view of shaft refinement

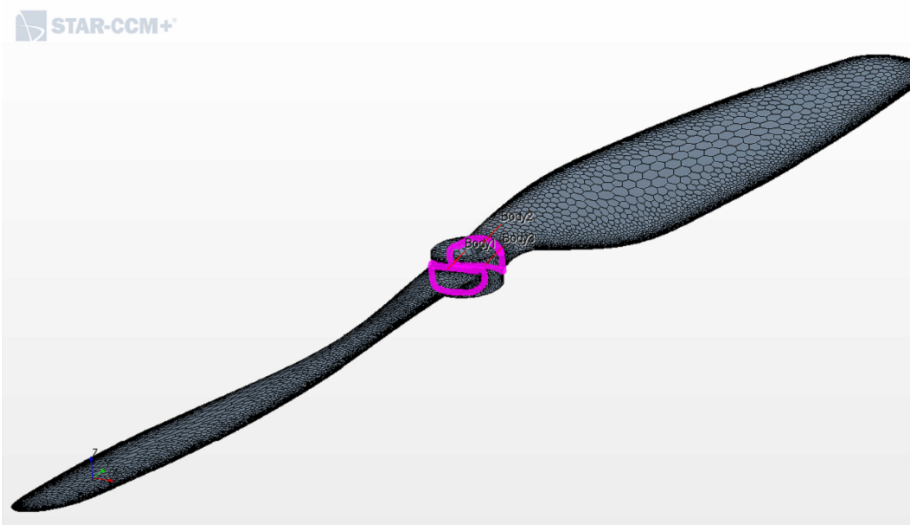

Figure 5.18: Isometric view of shaft refinement

At last it was performed a final set of refinement for an unique simulation with an ultra refined edge to capture as best as possible the edge of the propeller that have a blend radius of only 0.05 *mm* for his nature of thin profile. This last set is called "*Fine Ref*" and the simulation performed using also this set is the "*Dom4Fine*", a better description will be provided later.
For this last simulation were made a set of cylinder obtained as same as before, so using a sweep on the CAD software, but this time the diameter was of 0.1 *mm* to seizure the blend on the edge (5.19 and 5.20).

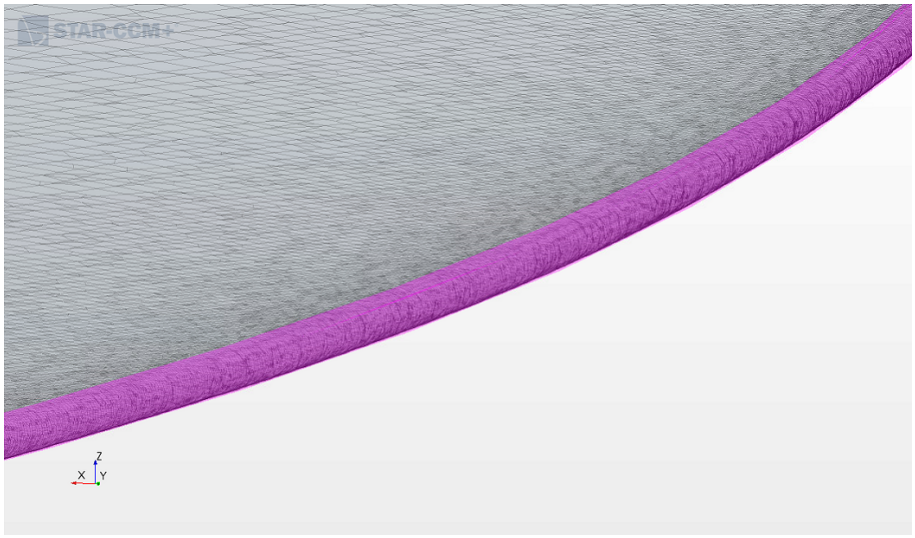

Figure 5.19: Fine edge refinement

Refinement	Low Edge Ref	Low and Edge Ref	All three sets
Number of cells	$1 \cdot 10^6$ cells	$4 \cdot 10^6$ cells	$17 \cdot 10^6$ cells

After first simulation was decided to not use furthermore the *Fine Ref* because the enhancement obtained is not worth enough compare to the increase of computational cost, so the simulations later described are all created with the only two firsts set of refinements. The cells amount obtained for the different rotational domain tests are described in the 5.6

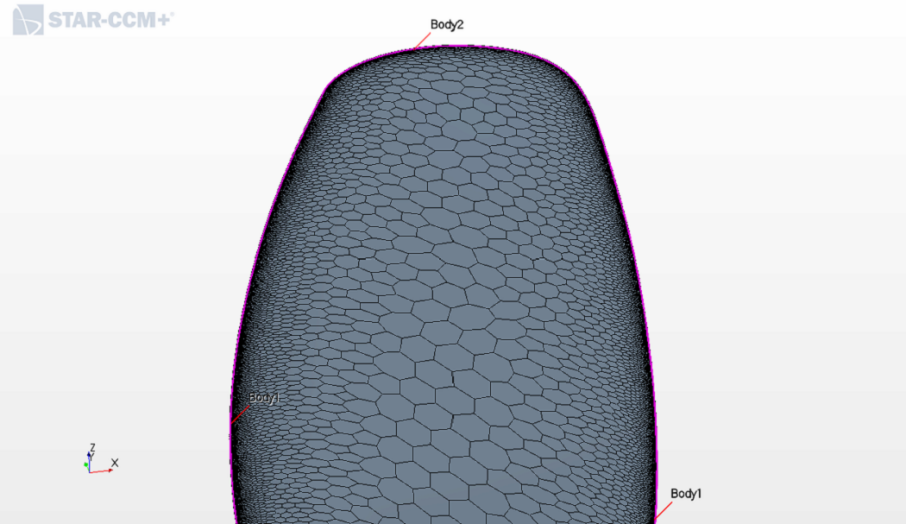

Figure 5.20: Top view of fine edge refinement

Rotational Domain	Number of cells
Domain 1	$1.9 \cdot 10^6$ cells
Domain 2	$2.3 \cdot 10^6$ cells
Domain 3	$2.5 \cdot 10^6$ cells
Domain 4	$2.7 \cdot 10^6$ cells

5.4.3 Optimum mesh chosen by comparative

To select the optimum mesh to use for further analysis it was made a comparative studying the different rotational domains and the different number of prism layer cells that are previously defined. As already says the *Fine Ref* is no more employ inside the simulations to enclose the computational cost.
Using four different rotational domains and a set of four different number of prism layer cells the total amount of simulations performed is sixteen, through these the entire mesh characterization is evaluated and grant a more wide look on the mesh interaction with the model.
Below are showed the comparison for the Thrust and Torque that are the main

results in which we are interested. These comparison are made using the software *MatLab* and generating for each of the curves a spline to better follow the results and to not obtain a broken line but a gradient through the entire change of slope of the curve.

Analysing the reports inside the simulations were created the trends below, a common tendency for both the figure is that increase the rotational domain diameter leads to an asymptotic results, this is clear into the Thrust trend, but even the Torque shows a similar movement.

This trend is simply explained, to create the simulation were created the rotational domain that is put in a rotatory movement, but this is only a representation of reality, instead the real physics is rotation of the propeller inside the air volume, so when the rotational domain diameter is increased gives a result more accurate and similar to the real one.

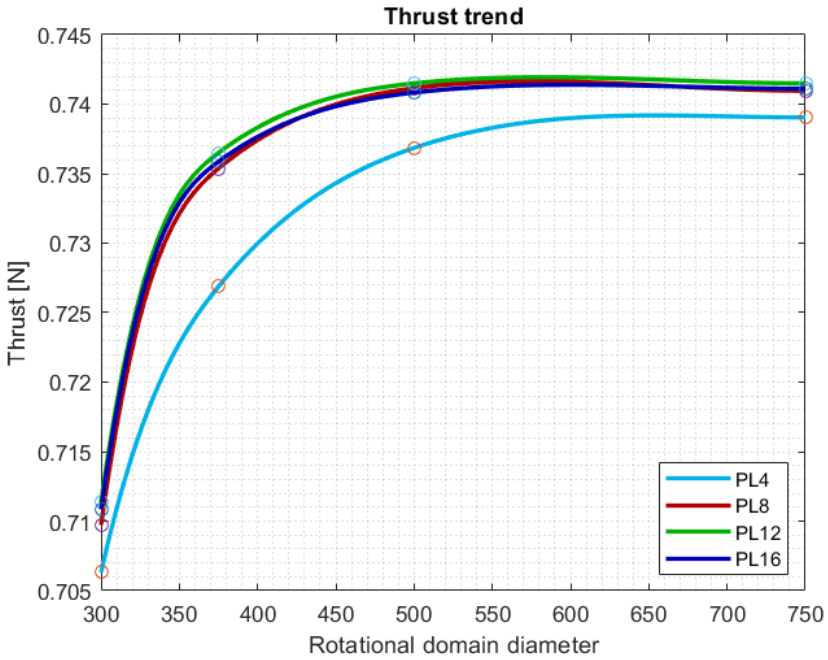

Figure 5.21: Thrust trend comparison

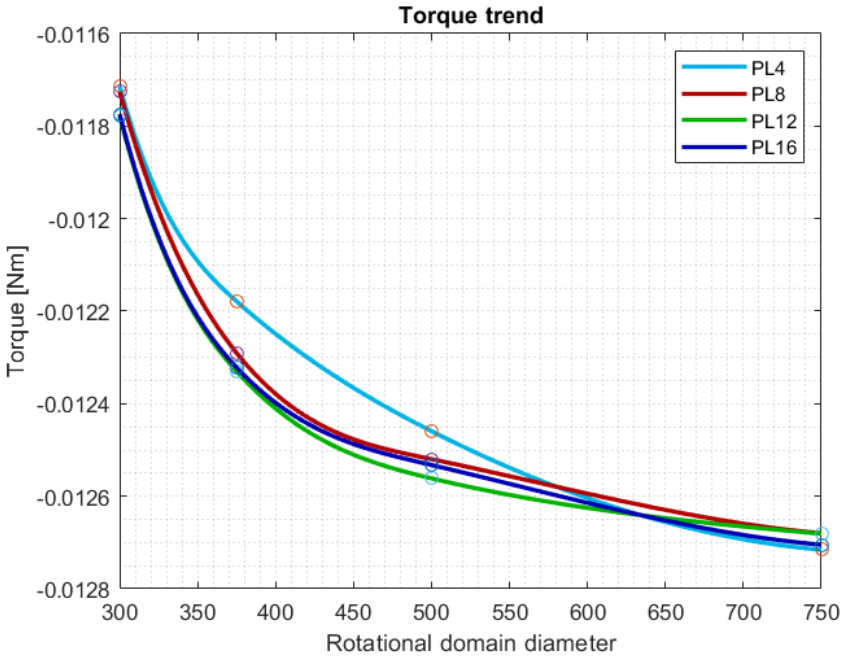

Figure 5.22: Torque trend comparison

A more careful view show how the increment of number of prism layer drive to condensed results spline so the improvement of the prism layer mesh exploit finer results, the answer to search is how convenient is to increase these two mesh parameters trying to get closer to the results without obtaining a mesh too massive.

To solve this question a important parameter is used, the $WallY^+$, using this is possible to understand if the boundary layer is fully enclosed and well discretized, for further explanation is suggested the read of the appendix, for this application is decided to take as acceptable value of $WallY^+$ one below 2 and is required the parameter to be as much uniform as possible.

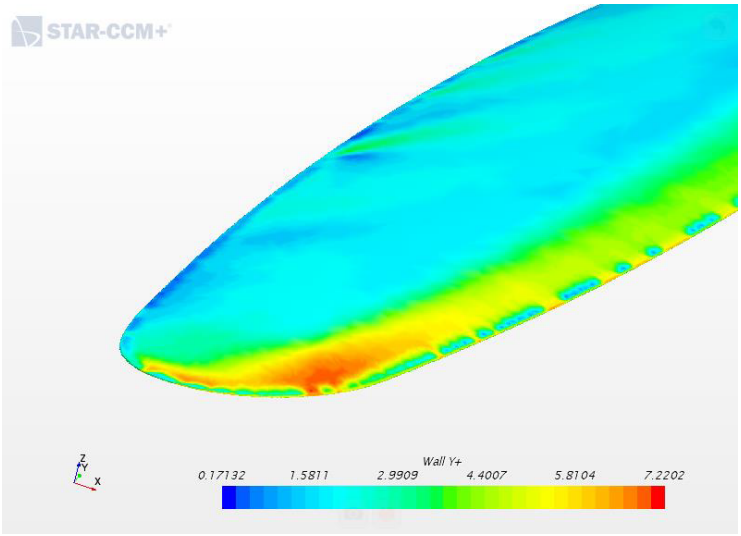

Figure 5.23: $WallY^+$ on propeller with PL4 mesh

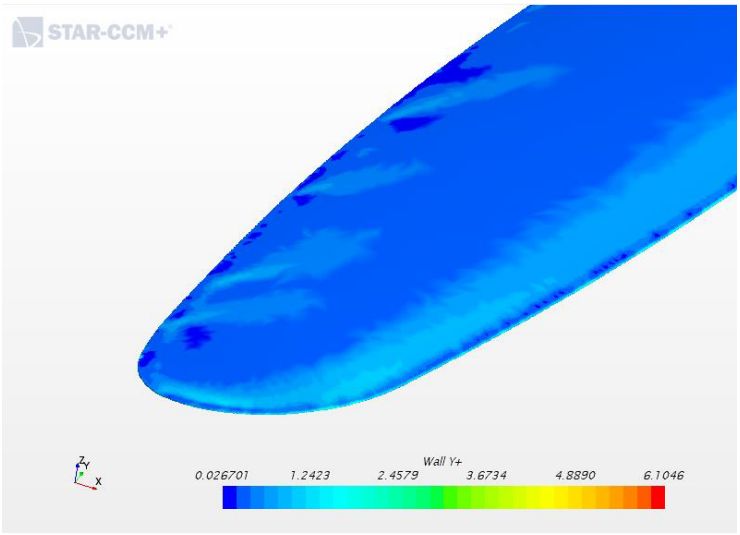

Figure 5.24: $WallY^+$ on propeller with PL8 mesh

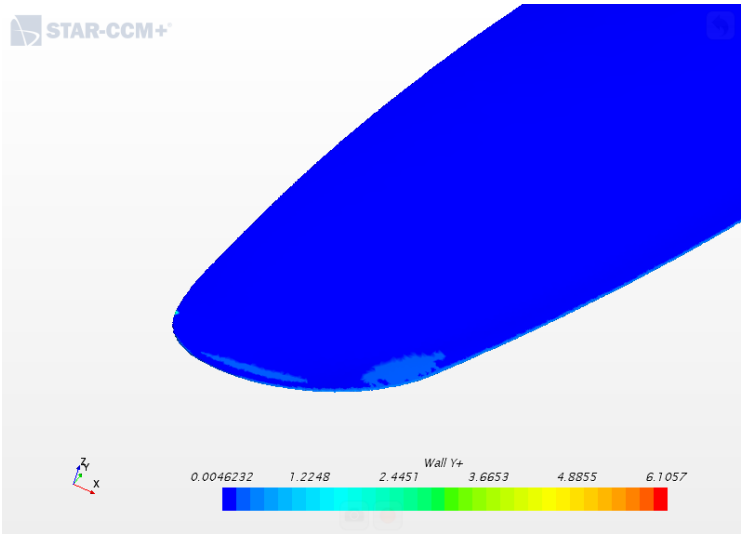

Figure 5.25: $WallY^+$ on propeller with PL12 mesh

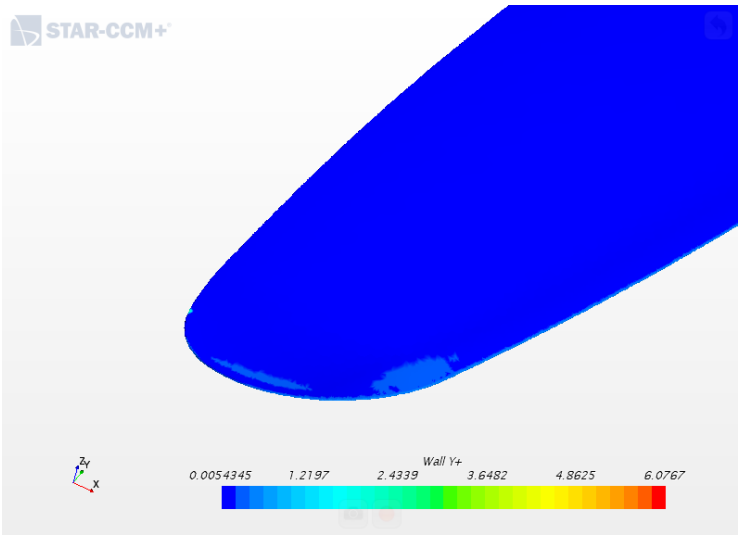

Figure 5.26: $WallY^+$ on propeller with PL16 mesh

Even if the parameter distribution in the last two cases is near to optimal, the maximum value of Y^+ is nearby to 6, a really high value, this is locate in one point at trailing edge as a spike on the mesh. These two restrictions cut the feasible solutions eliminating the sets with 4 and 8 layers of prism layer for every rotational domain. To guide us to the choice of the number of layers inside the prism layer were created two different graphs, these are made thinking as the *PL16* was the set of simulations with an higher level of accuracy, so for each results was evaluated the deviation from the $PL16$ results obtaining the fig. (5.27 and 5.28).

Looking at these as proof of the exclusion of $PL4$ is clear of the higher deviation from the more accurate set of simulations, but a further sight to the other two cases shows that the results are really close to each other and to the $PL16$ results, with a deviation near the 0.2%. As the rotational domain chosen is the bigger because the number of cells of the mesh do not change from a 500 mm to a 750 mm, the exactly same reasoning is applied to the choose of the $PL12$ because the number of cells grows about half a million, but comparing to $PL8$ the results are bond to a non uniform $WallY^+$.

The $PL16$ is not chosen because the mesh still grows, but this happens without any improve of the $WallY^+$ or any substantial different results. So the mesh chosen for the following simulations is the one with rotational domain diameter of 750 mm and a number of layers inside the prism layer of 12, also called *4PL12*.

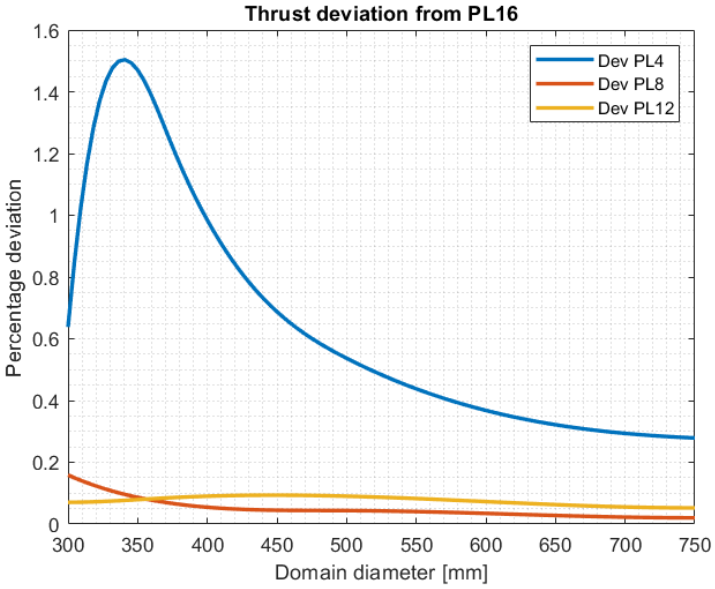

Figure 5.27: Thrust results deviation from PL16

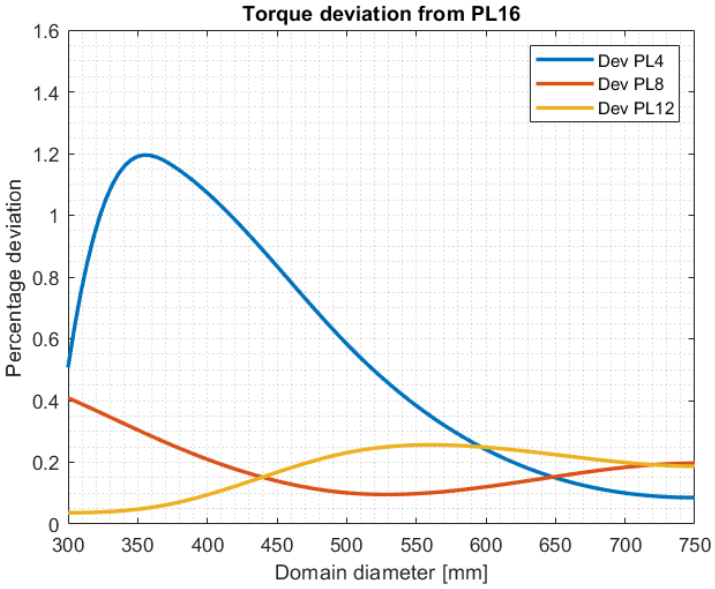

Figure 5.28: Torque results deviation from PL16

5.5 Validation

The previous work alone is meaningless if is not attached to the validation of results obtained through a comparative with experimental data.
To achieve a validation of the activity are feasible few different paths, for example one of these is to produce the propeller in exam by plastic molding and after balanced it will performed a physical analysis using a load cell to obtain the Thrust data and the Torque of the propeller, these data can be compared to the computational results as a validation of the model.
Another path, the one we chosen is to analyze a CAD model of which the experimental data are already given, so using a Replace Part inside $StarCCM+$ it will be used the exactly same simulation with the same parameter of the mesh, but are necessary to calculate a new mesh to execute the simulation. The propeller chosen was the $8x3.8$ Slow Flyer and for this propeller the experimental data obtained from the [10] are transposed into *MatLab* obtaining a curve of Thrust and Torque.
Inside the simulations for the validation where used the rotational domain diameter of 750 mm and then positioning at 2500 rpm, as the other simulations performed, are computed three different simulations modifying the number of layer of the prism layer, this can lead to a better comprehension of the error inside the computational results. As shown inside the graphs fig.(5.29 and 5.30 is easily visible the 5% error bar used to understand if the results are inside a 5% of error, the circles are the experimental and computational results. Looking at these figures is clear that even the results obtained with $PL4$ is still inside the feasible error, but compared to the other the absolute error can be halved using a finer mesh. For a better visualization of the reduction of the error were plotted the trend of the thrust error and of the torque error fig.(5.31 and 5.32), in these two graphs are without doubt visible the tendency of the results to approach the experimental result due to the increase of the number of layers of the prism layer.

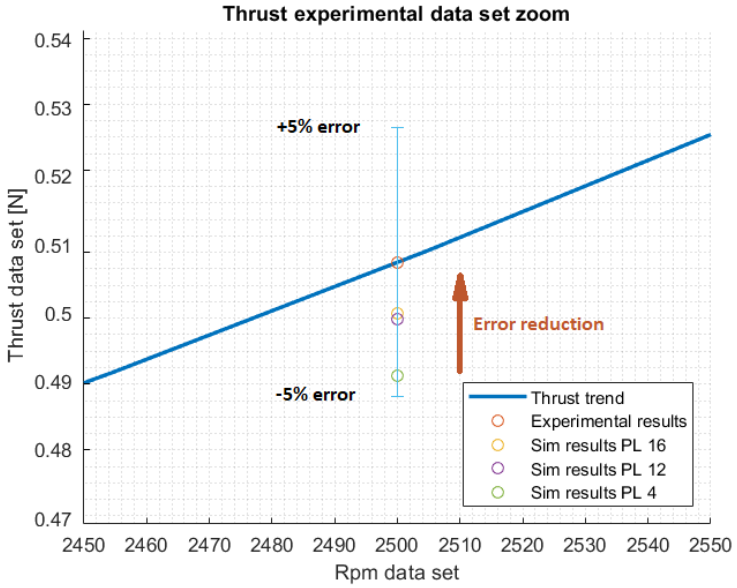

Figure 5.29: Thrust computational deviation from experimental data

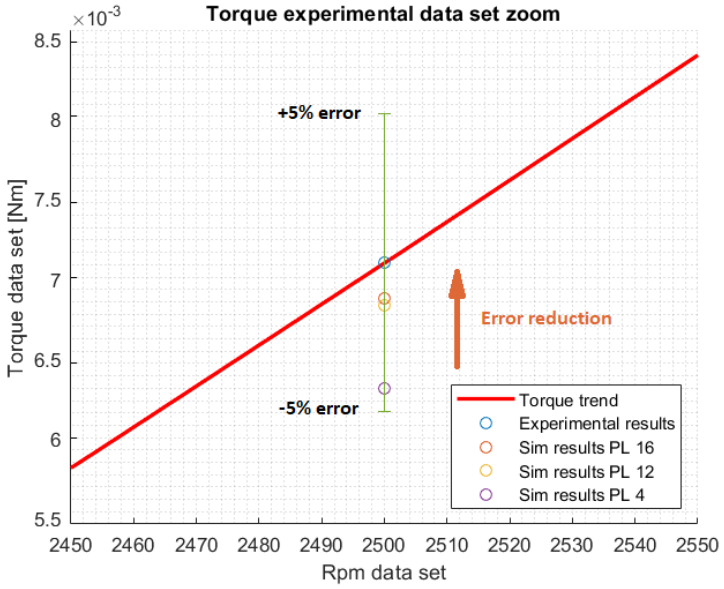

Figure 5.30: Torque computational deviation from experimental data

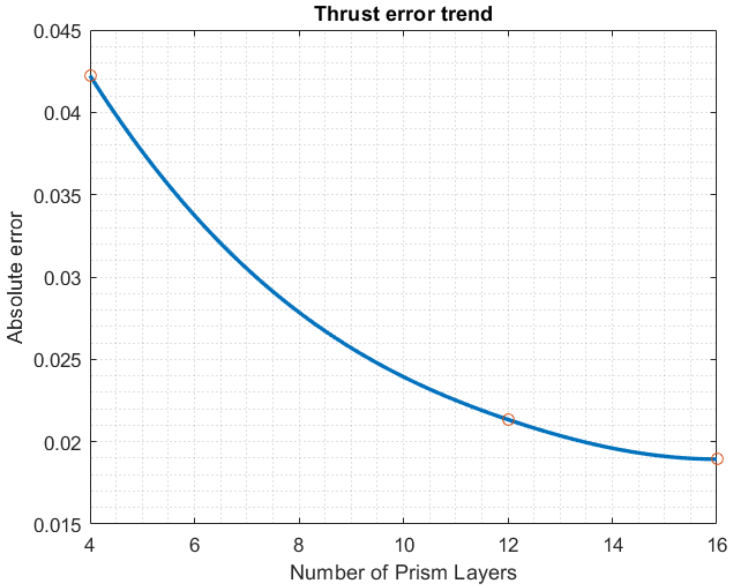

Figure 5.31: Thrust deviation error

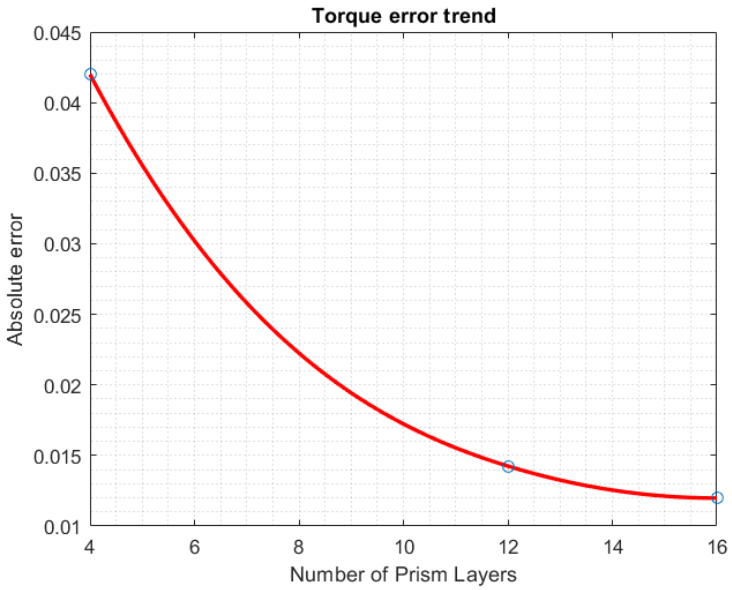

Figure 5.32: Torque deviation error

5.6 Changing geometry

At last because the $WallY^+$ always present a spike on the geometry is decided to try to eliminate this hot spot trying to lightly modify the geometry, indeed to achieve this it was changed the edge fillet radius from 0.05 mm to 0.5 mm. To perform another simulation are used the mesh parameters chosen previously or rather rotational domain diameter of 750 mm and prism layer with 12 layers.
The generation of this new mesh needed a new set of refinement and to achieve a good discretization of the geometry are always used the mesh value antecedent used.

	Number of cells
Base geometry	$3.8 \cdot 10^6$ cells
Modified geometry	$5.2 \cdot 10^6$ cells

As shown above the new geometry require an increase of 37% of number of cells of the mesh, but here the things makes interesting, this new geometry grant a colossal reduction on $WallY^+$ with an increase of number of cells that is iniquitous compared to the enormous increase needed to obtain the same $WallY^+$ reduction with the old geometry. At a untrained sight the new geometry as a less uniform $WallY^+$, but looking at the legend is clear that the new maximum value is near ten times lower with a maximum of 0.57. The results obtained from the two different geometry are compared with a 5% of deviation so the difference is not negligible. Due the optimal $WallY^+$ values this new geometry is chosen to be used as the starting geometry to further modify in the next chapter.

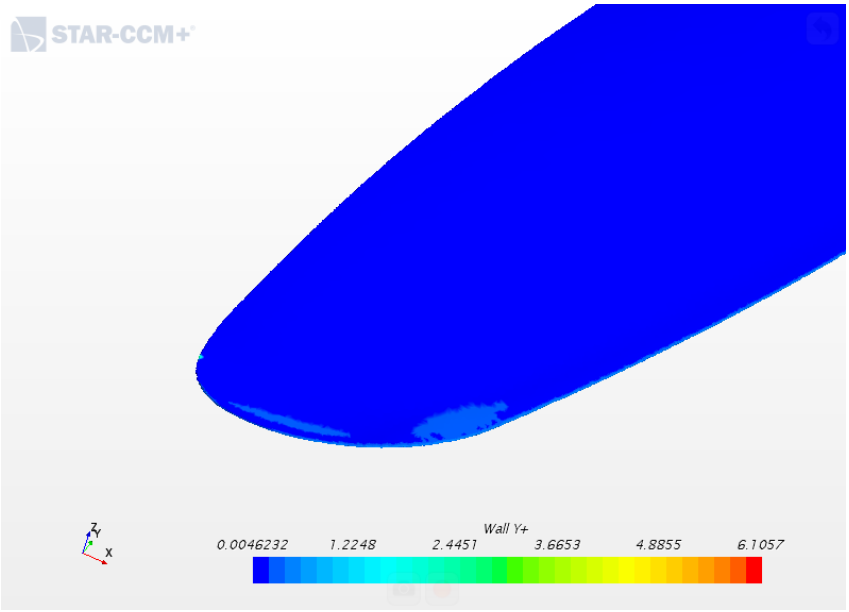

Figure 5.33: $WallY^+$ on old propeller with PL12 mesh

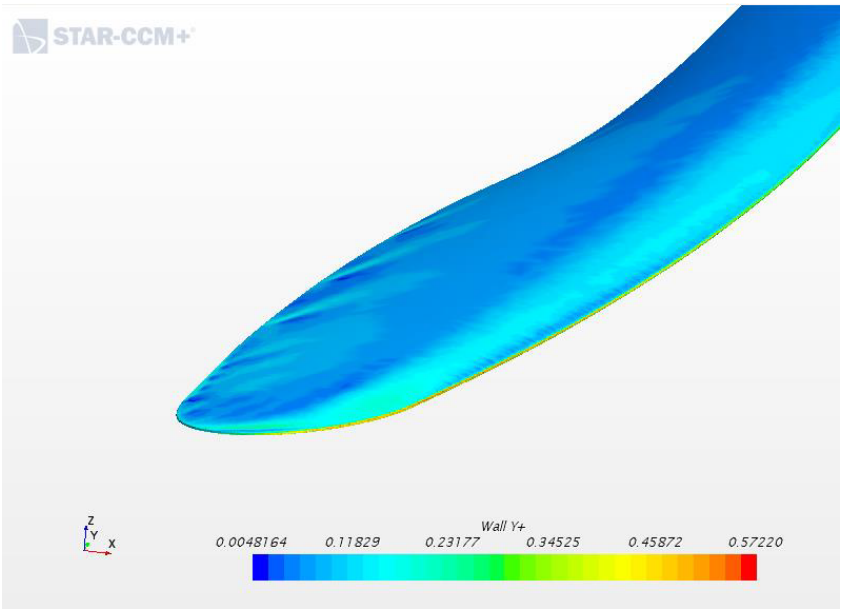

Figure 5.34: $WallY^+$ on new propeller with PL12 mesh

Chapter 6

Thrust optimization

The last stage of this work is about a thrust optimization performed through a twist analysis. To execute this analysis was mandatory to start from the simplest case analyzable, so it was chosen to perform a 2D simulation campaign on a set of propeller airfoil.
After some analysis for each airfoil it was determined a twist optimum and then used to modify the 3D geometry of the propeller to finish through a last 3D simulation of the complete propeller to compare the new performance with the old ones.

6.1 2D analysis

Studying the 3D propeller CAD is noticeable that is obtained using nine different airfoil as base for the extrusion of the surface, in this section of the thesis was chosen to execute the thrust optimization for only four of the airfoil, the even ones, this to assure a quicker analysis without lose coherence and the continuum of the propeller, which that can be happened if from a station (position of one of the nine base airfoils) to another the twist angle were changed too much.

So at the chosen stations the airfoils were extrapolated and to grant an optimal geometry characterization they were scaled of 10 times, without this operation the airfoil geometry would have been lost due the small dimension (fig. 6.1).

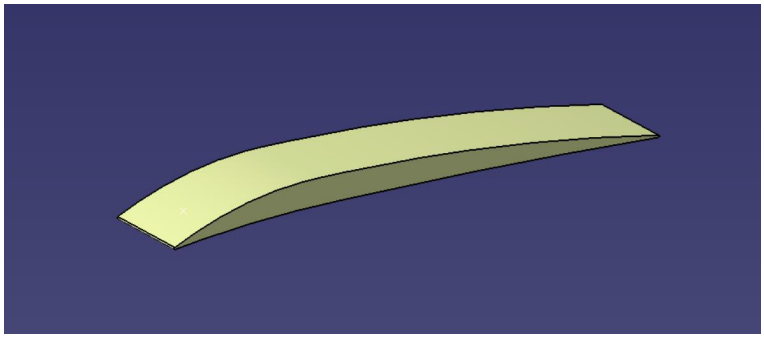

Figure 6.1: Catia view of station airfoil scaled

After this operations performed in *Catia* the entire geometry was transferred to *Star CCM+* with an Import geometry, then it was created a Wind Tunnel where analyse every airfoil at the various twist angle.

6.1.1 Mesh

The wind tunnel and the geometry were 3D, but using the function *Badge for 2D mesh* were possible to set a 2D analysis. Wind tunnel dimensions are 100 mm of height and 20 mm of width and the airfoil leading edge lay in the first 2 mm of the tunnel. The mesh parameters for the 2D mesh used are a Base Size of 2 mm with a Target Surface Size of 1 mm, these two are slightly smaller than the previous used, but for a 2D mesh is conceivable to use finer mesh without weighing on computational cost. Instead for the Prism layer mesh the parameters are quite standard and similar to the old ones used into the 3D simulations, indeed were used a 0.5 mm of Prism layer thickness and using a Stretching of 1.5 are settled 12 layers.
To achieve a acceptable degree of accuracy for the results were set four different layers of mesh refinements (fig. 6.2 and 6.3).

- Ref Block: this box was created to be a first refinement that the flow has to encounter while is approaching the airfoil, this is 35 mm wide and 20 mm tall, with a 0.2 mm mesh size.
- Ref Offset: a box smaller than the previous one, but in this case is twisted of the same angle of the airfoil, mesh size of 0.05 mm.
- Tail: for this was chosen to use a triangle shape, the edge is on the first fourth of airfoil and ends 45 mm back with a base of 40 mm, this is with a mesh size 0.1 mm.
- Edge Ref: at trailing and leading edges were created two boxes of 1 mm of dimensions for better envelope the edges with a 0.01 mm of mesh size.

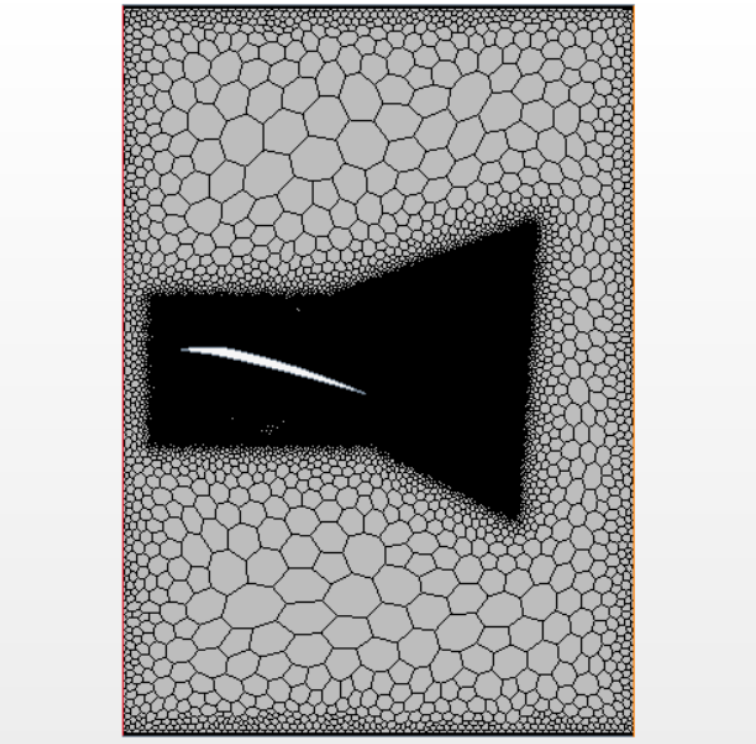

Figure 6.2: Overview of the 2D mesh

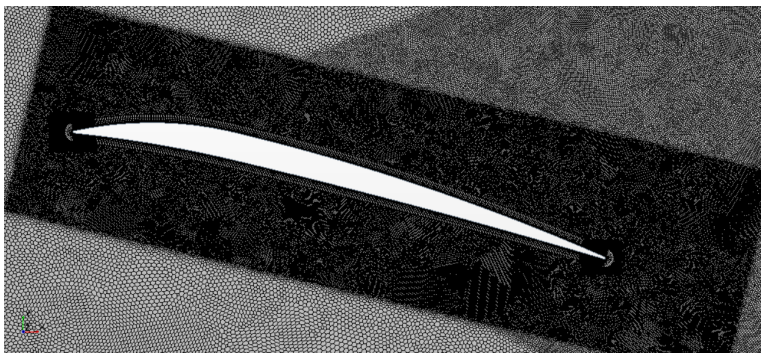

Figure 6.3: 2D mesh zoomed

6.1.2 Physic

To set the simulation physic to be comparable to the 3D simulation were decided to calculate the velocity at each station knowing which rotational speed is used at the 3D simulation, so combine this information with the radius of each station.

Using the previous 2500 *rpm* as rotational speed of the propeller is easily obtained the following

Station	Radius $[mm]$	Velocity $[\frac{m}{s}]$
0.2 R	25.4	6.65
0.4 R	50.8	13.3
0.6 R	76.2	19.95
0.8 R	101.6	26.6

To earn a good comparison from 2D and 3D in addition to the airflow velocity was decided to use the angle of attack observed in the 3D simulation as the airflow direction and it was imposed using a vector field function, and the angle obtained are [12 5 1 1].

After a first simulation used as benchmark for the transfer from 3D to 2D, for each station were performed a set of 6 simulations, with variable twist, this was modified from a simulation from another using a rotate transformation and the value used are not always the same due the different Thrust and Drag trend.
In the end only the Thrust report was used to chose the optimum of twist angle, and this thrust report was reach with a Statistics Report of the last 150 iterations for a stable result (fig 6.4).

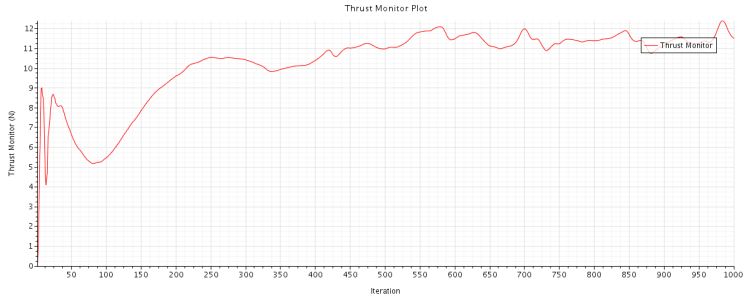

Figure 6.4: 2D typical thrust plot

Using the software *Matlab* were plotted the trends obtained from the simulations, after a total of 28 simulations were realized the following plots.

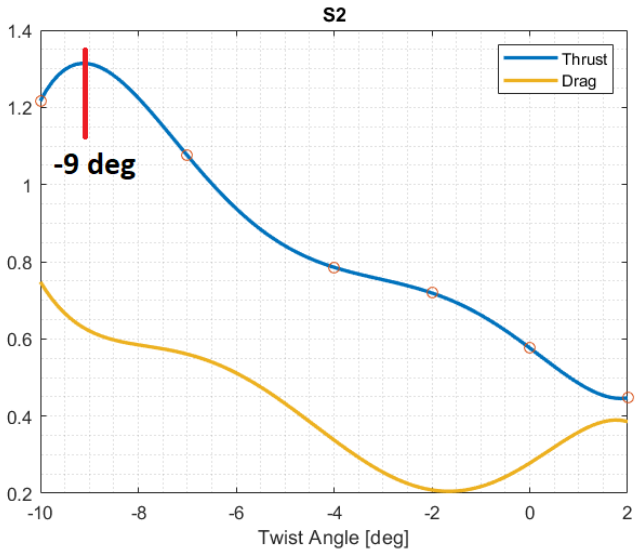

Figure 6.5: Station 2 Thrust and Drag trends

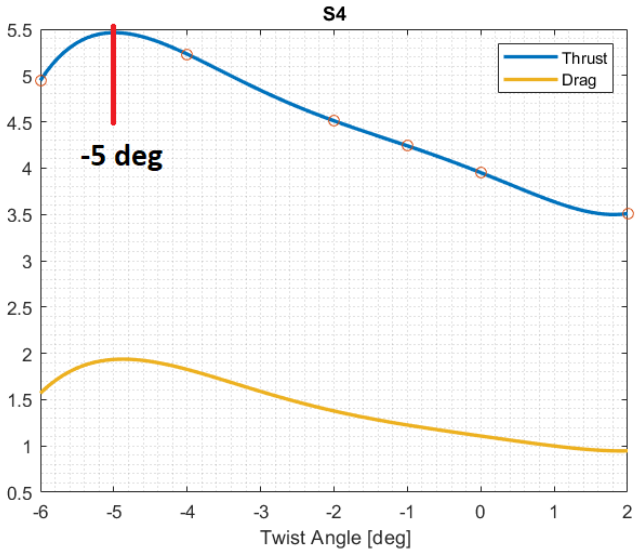

Figure 6.6: Station 4 Thrust and Drag trends

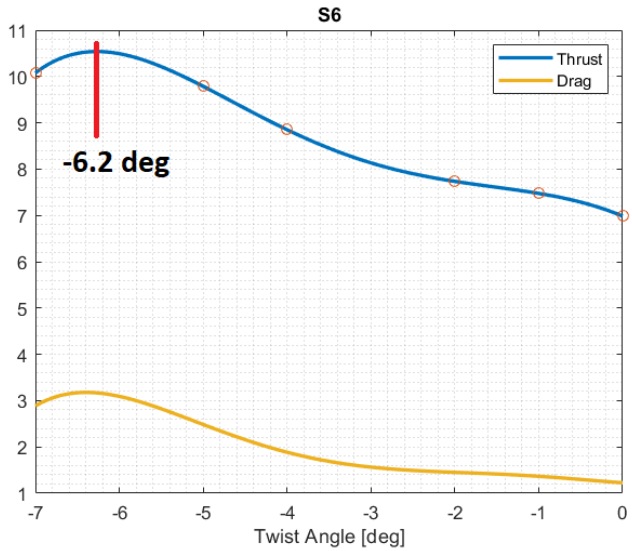

Figure 6.7: Station 6 Thrust and Drag trends

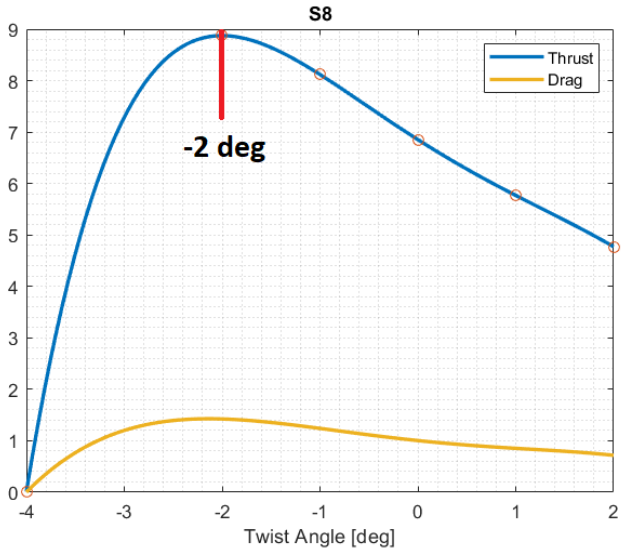

Figure 6.8: Station 8 Thrust and Drag trends

The new twist angle gains a mean thrust increase of near 60 %, that is quite big improve, but is important to remember that this increase is for a pure 2D analysis and only for four section of the propeller, so is presumable that switching to a 3D case the increase will be reduced due the continuum geometry and the birth of all the types of 3D phenomena as vortex and finite wing phenomena. Moreover this type of analysis isn't quite realistic due the impossibility of schematic a rotational physics into a 2D domain.
To ensure that the 2D simulations were well placed was mandatory to verify that the oscillation in the thrust for a single airfoil was observable even if the simulation was in 3 dimensions.

6.2 3D analysis

After the simulation campaign implemented in the 2D analysis were reached the optimum of the twist angle for the 4 stations in exam, so the next step was to modify the 3D propeller geometry and this was made coming back to the CAD (fig 6.9).

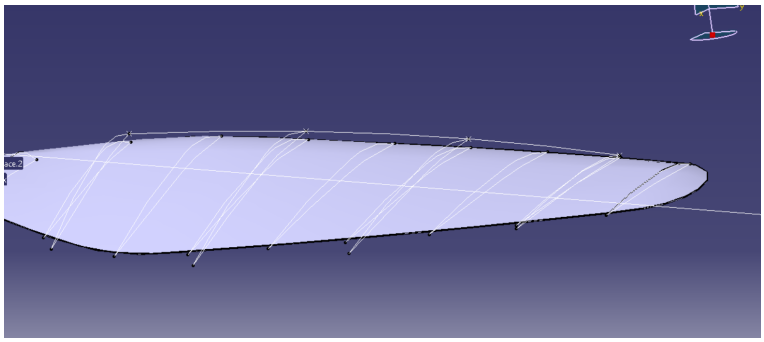

Figure 6.9: Geometry optimization

As already said, this analysis was far from perfect, but anyhow can be a interesting way to try to obtain confidence with a simple propeller optimization. The simulation setting of the new propeller 3D analysis were the same of the

ones chosen at the last of the previous chapter so all the mesh parameters and refinement are defined and better described previously.
Looking at the pressure and velocity fields for each station is easily identified that the differences between the two propeller are quite small, however even with a simple analysis far from perfection was found an improvement to the characteristics of the propeller.
Talking about the pressure differences between the same stations in different propellers

- Station 3, from 6.10 to the 6.11 is visible a new pressure 'bubble' formation, that mean a lower pressure on the top side of propeller so an higher velocity.
- Station 5, like before and for now on will be always an lower pressure on the top of propeller 6.11, but this time is distinguishable how the pressure is lower for much long time, approaching the trailing edge the pressure maintain low values.
- Station 6, in 6.15 is noticeable bigger 'bubble' over and under the propeller unlike 6.14.
- Station 7, again is clear that over the propeller there are more pressure 'bubble'.

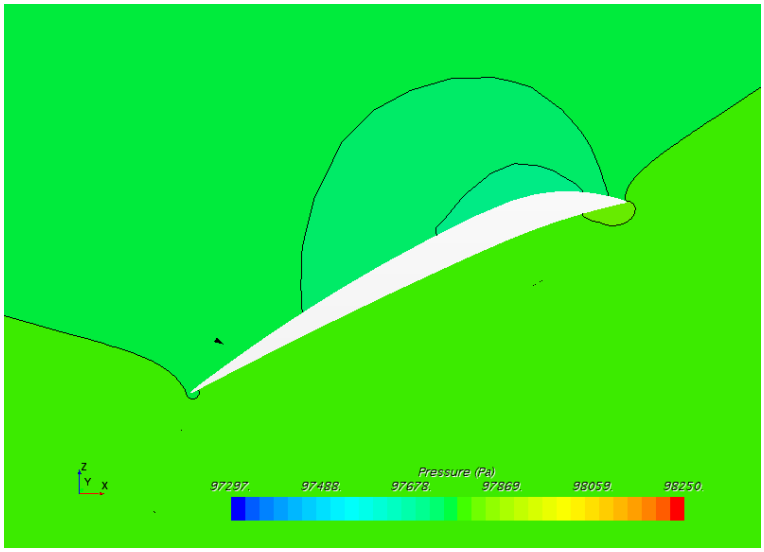

Figure 6.10: Station 3 pressure for old propeller

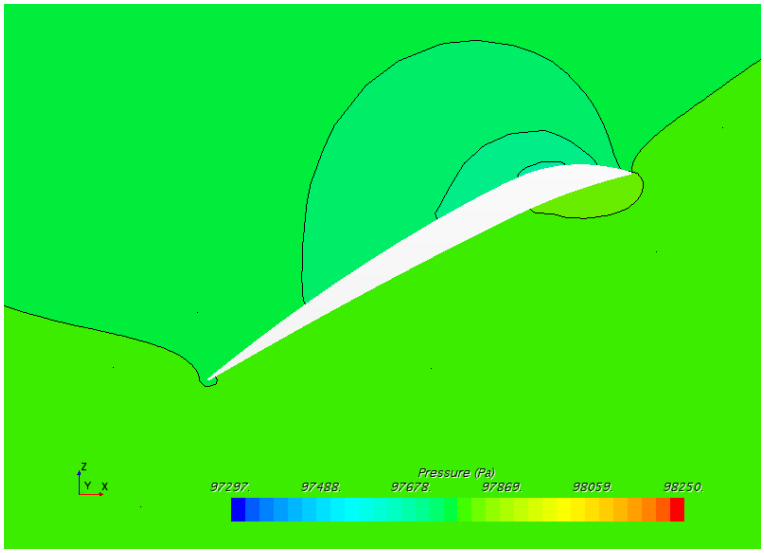

Figure 6.11: Station 3 pressure for new propeller

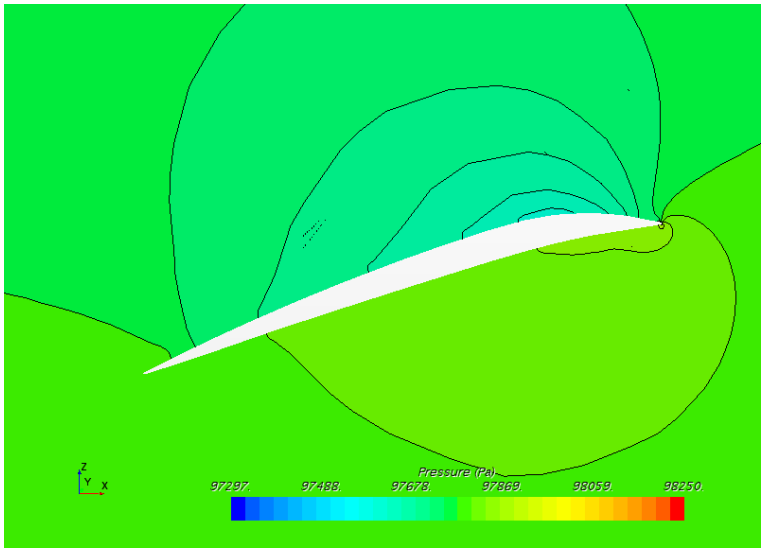

Figure 6.12: Station 5 pressure for old propeller

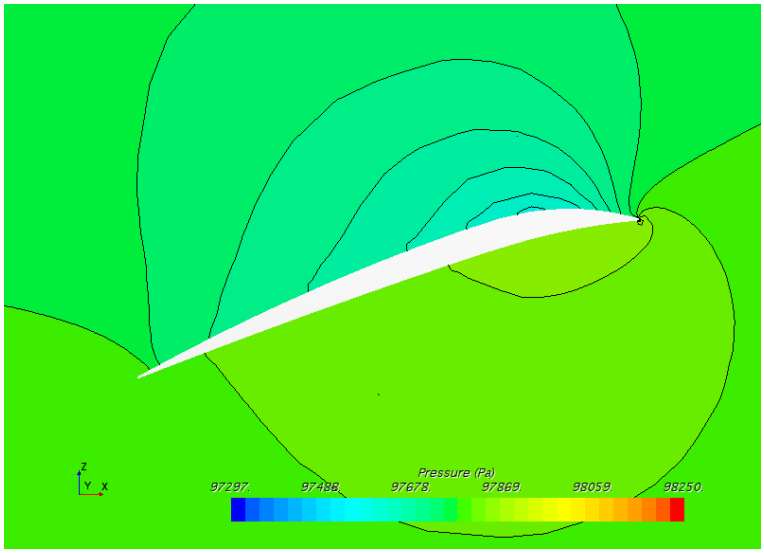

Figure 6.13: Station 5 pressure for new propeller

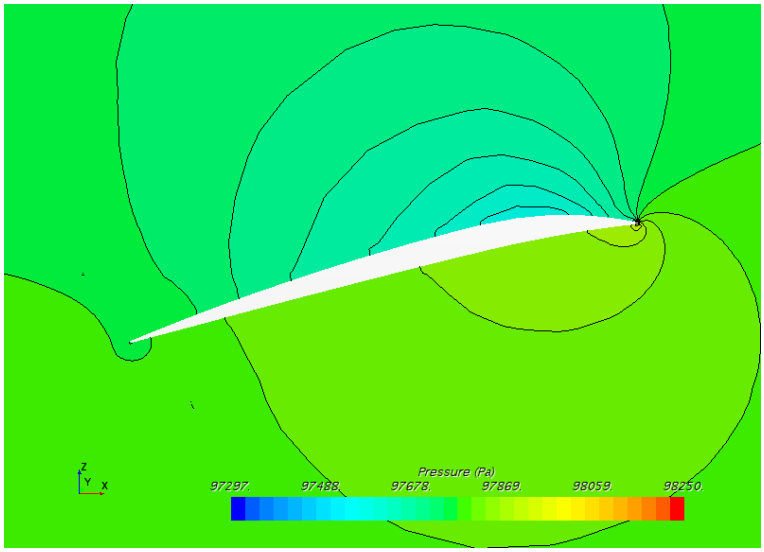

Figure 6.14: Station 6 pressure for old propeller

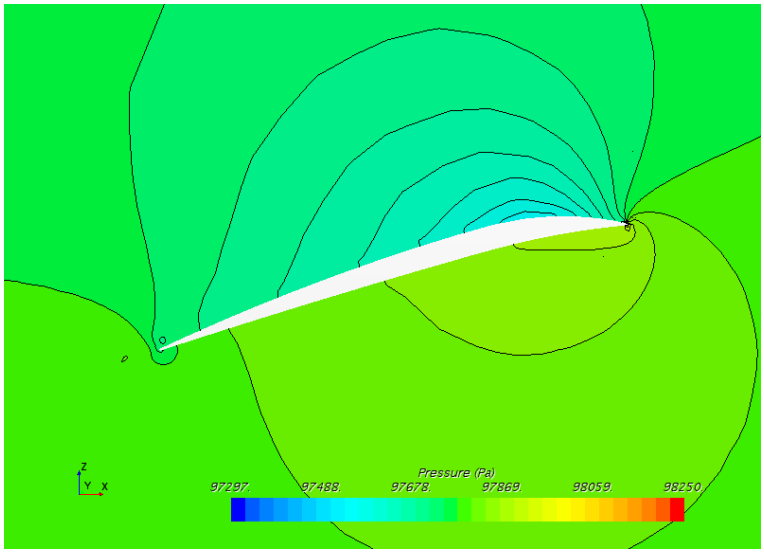

Figure 6.15: Station 6 pressure for new propeller

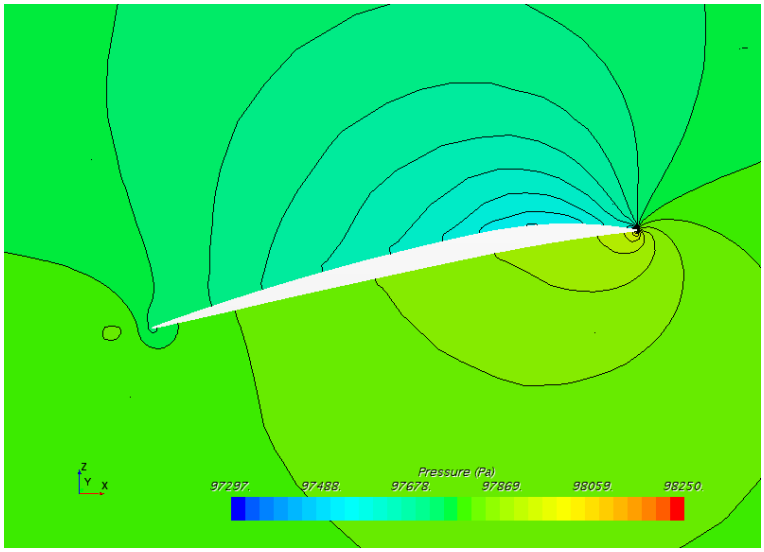

Figure 6.16: Station 7 pressure for old propeller

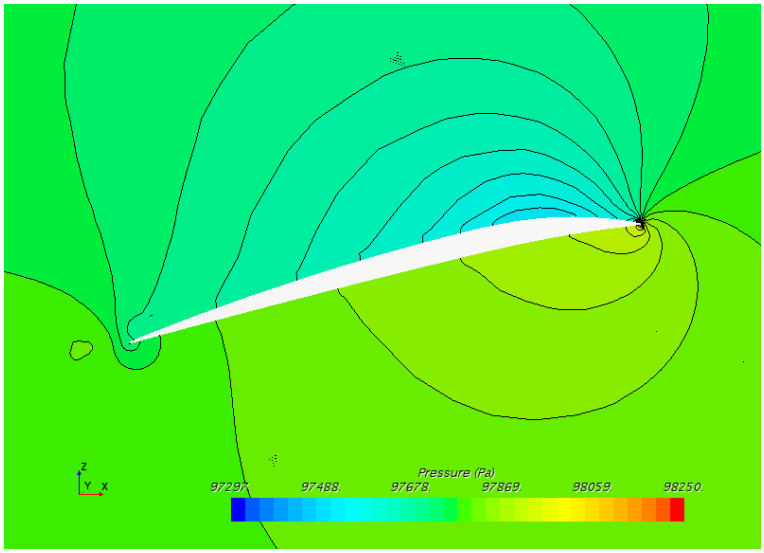

Figure 6.17: Station 7 pressure for new propeller

For velocity post processing analysis are chosen some different stations, but again are possible some comments.

- Station 3, here from 6.18 to 6.19 is visible the same velocity remains till the trailing edge.
- Station 4, in 6.21 is discernible a smoother velocity profile over and under the propeller.
- Station 5, looking at 6.23 unlike 6.22 is evident an higher rear propeller velocity.
- Station 6, again in this station is discernible a greater velocity at the trailing edge.
- Station 9, at last in this station 6.26 and 6.27 is detectable a clear difference of velocity between the two propellers.

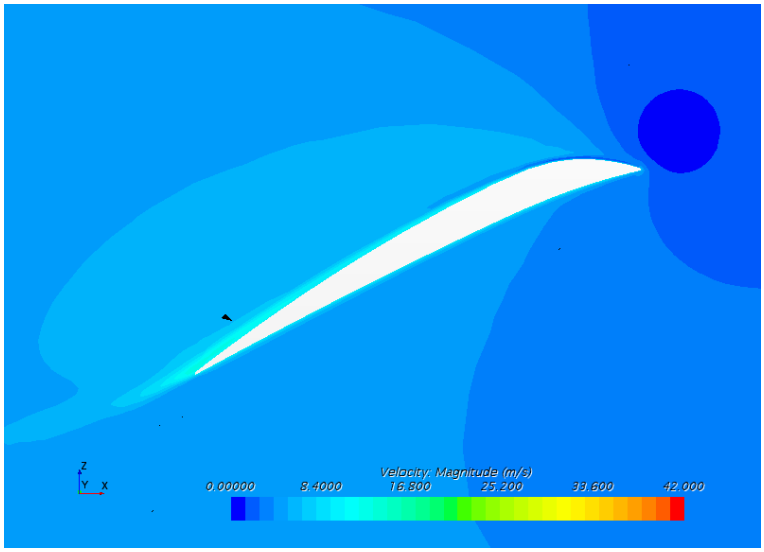

Figure 6.18: Station 3 velocity for old propeller

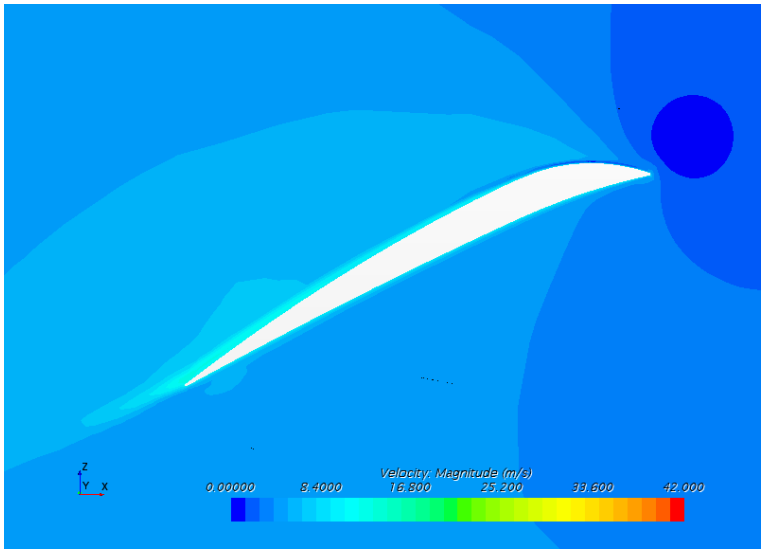

Figure 6.19: Station 3 velocity for new propeller

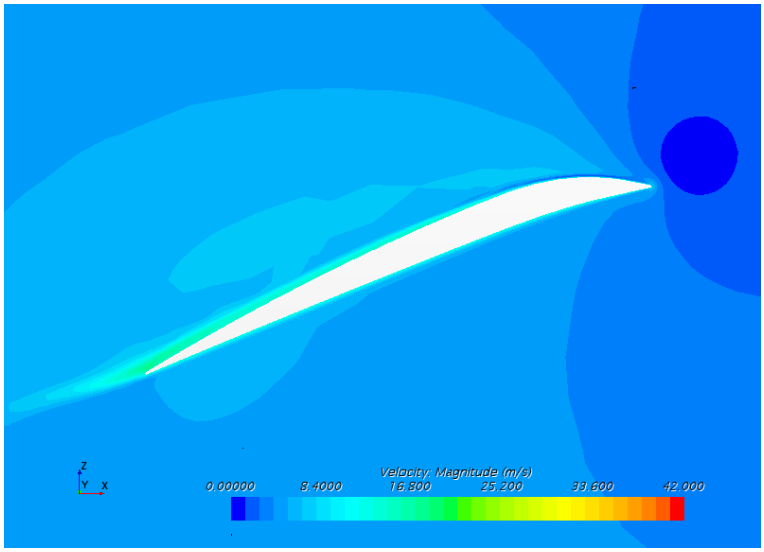

Figure 6.20: Station 4 velocity for old propeller

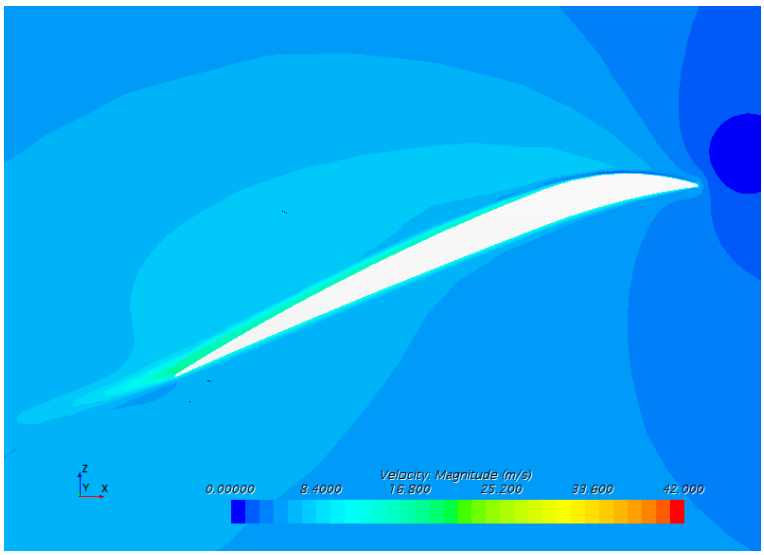

Figure 6.21: Station 4 velocity for new propeller

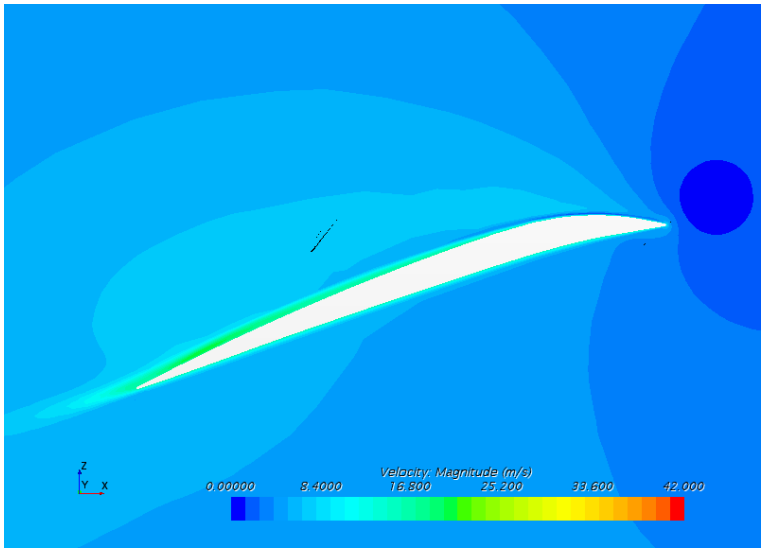

Figure 6.22: Station 5 velocity for old propeller

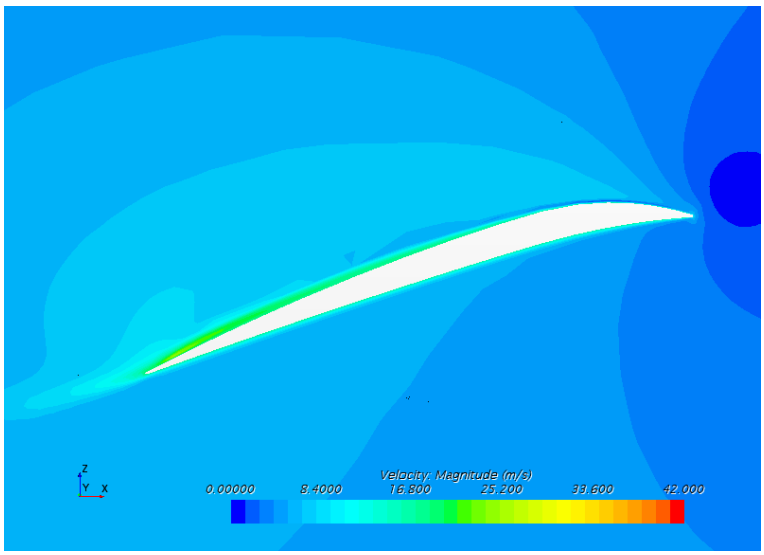

Figure 6.23: Station 5 velocity for new propeller

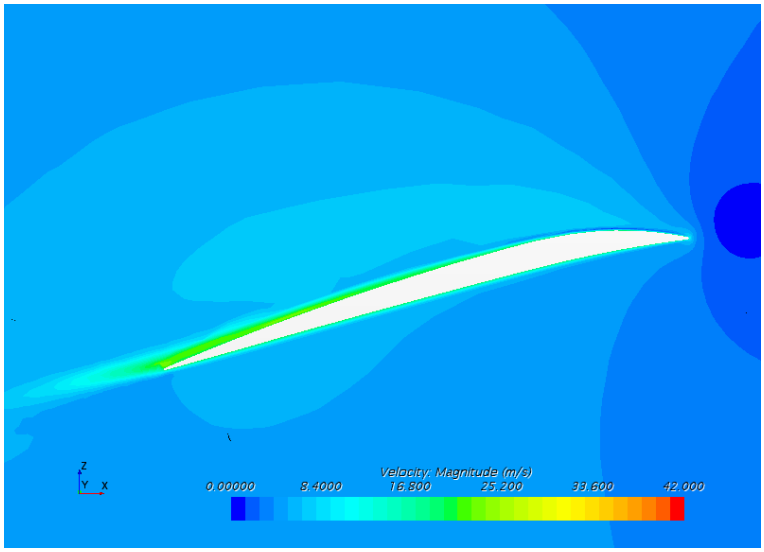

Figure 6.24: Station 6 velocity for old propeller

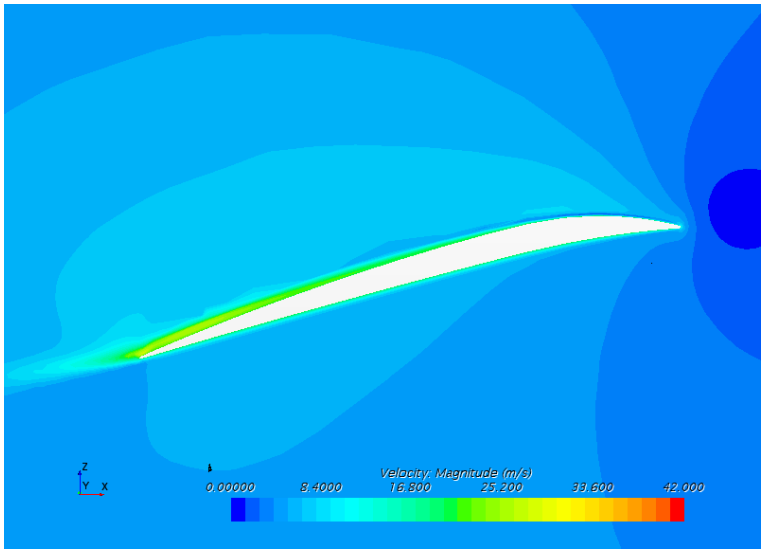

Figure 6.25: Station 6 velocity for new propeller

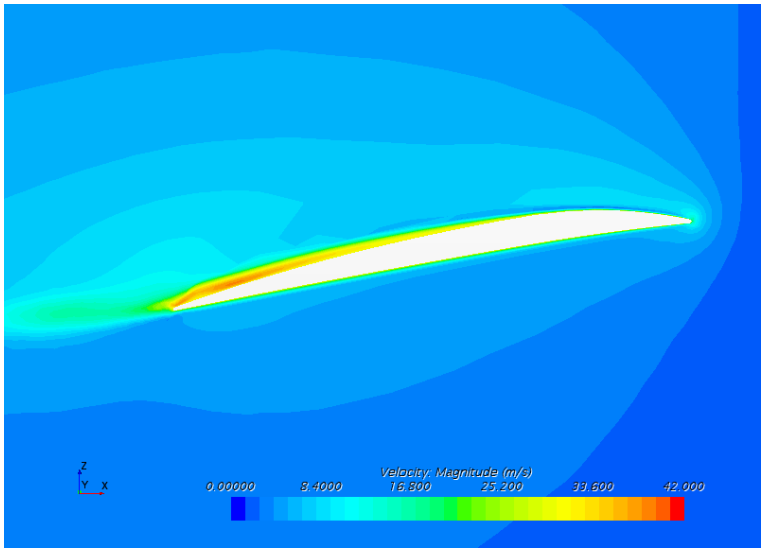

Figure 6.26: Station 9 velocity for old propeller

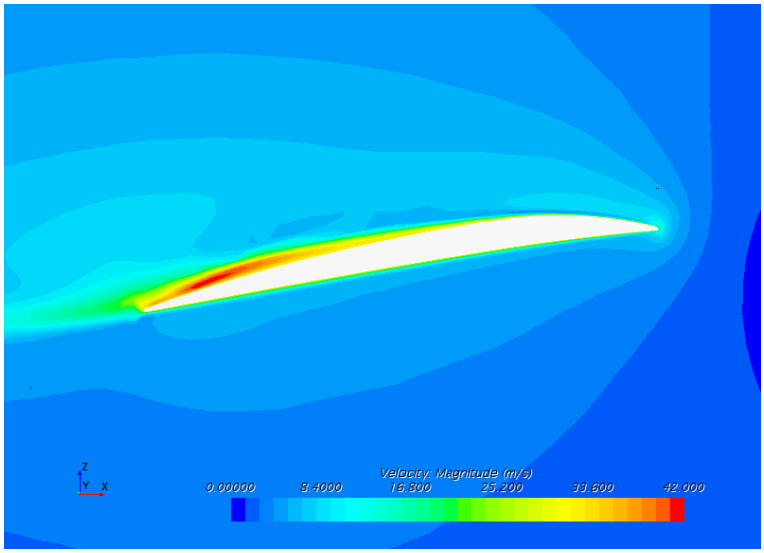

Figure 6.27: Station 9 velocity for new propeller

These figures allow to see the differences in terms of pressure and velocity that are achieved by the geometry optimization. In the end are compared Thrust and Drag reports to understand the improvement that is achieved by this optimization and the results of this optimization is clear with the next table.

		Delta percentage
Old Thrust $[N]$	0.74111	+6.67%
New Thrust $[N]$	0.79056	
Old Torque $[Nm]$	0.01270	+10.56%
New Torque $[Nm]$	0.01405	

First thing coming up to us is that the thrust increase is a tenth of the thrust boost previously obtained in the 2D analysis, but as already said a similar drift was predicted assuming the presence of 3D phenomena and due the switch from 2D airfoil to 3D continuum propeller.

The result is aligned to what is expected, after all only one parameter was modified during this thesis, so is feasible that working on more parameters can repay with an additional improvement for the report in exam. To be clear the further development must be achieved only through an 3D geometry optimization due the method used in this thesis is too simplified and cannot embrace all the sides of a multi parameters optimization.

Conclusion

In the end just summing up all work done until here, as it was the first step of a bigger project was mandatory to achieve a solid confidence with the software and the generation of an optimal mesh for the analysis case. So after a general study of the software was investigated the mesh generation, this with a trial and error process so the mesh parameters needs to be used in the optimization simulations were obtained through a simulation campaign.
To validate the system was performed a simulation and it was compared with results obtained in laboratory, this to understand how near the results can be with the simulation parameters chosen. At last a first test of optimization was executed, the 3D case was simplified and the optimization was evaluate in the 2D space and then an early improve of propeller geometry was proposed and analyzed with positive results.
To proceed in the project all initial steps have therefore been taken so after these presumably next is up to chose different geometry parameters and some boundaries to generate an optimization campaign through the utilization of software like *Siemens HEEDS* capable of managing optimization method such as gradient descent method.
This first solution of static hovering can be achieved with the mesh parameters obtained during this dissertation, but to further improve the geometry can be analyzed the propeller during the flight using the mesh overset briefly described before. This advanced method can grants to obtain a full flight envelope of the propeller that will enhance the problem simulation and relative analysis.

Appendix A

Wall Y^+

Before World War II nobody could write an equation to describe exactly how velocity behaves in the near wall region or far away from the wall, this until Prandtl, normalized the axes into y^+ (the axis that used to be the distance) and u^+ (the axis that used to be velocity).
The result on this work was that all the data sets experimental and calculated perfectly matched. In Computational Fluid Dynamics, the equation resulted from this work is still used as a function to figure out the shear stress at a wall node.

A.1 Why using wall functions?

Turbulent flows are everywhere in CFD and are significantly affected by the presence of walls, because the viscosity-affected regions have large gradients in the solution variables. Have an accurate representation of the near wall region grant a successful prediction of wall bounded turbulent flows.
Some turbulence models such as k-ϵ are only valid where the turbulence is fully developed, and do not perform well in the area close to the wall. To deal with the near wall region, two ways are usually proposed.

- One way is to integrate the turbulence to the wall. Turbulence models are modified to enable the viscosity affected region to be solved with the mesh down to the wall, including the viscous sublayer. When using a modified low Reynolds turbulence model to solve the near-wall region, the center of the first must be placed in the viscous sublayer region (near $y^+ = 1$, but are required a large number mesh cells. Thus, an abundant computational resources are required A.1. Usually are used a low-Re model like $k - \omega$ and this method is good when you are interested in the forces on the wall.

- Another way is to use the so-called wall functions, thee ones can model the near wall region. Wall functions are empirical equations used to satisfy the physics in the near wall region. With this method the first cell center needs to be placed in the log-law region to have accurate results. Wall functions were used to bridge the inner region between the turbulence fully developed region and the wall. When using the wall functions method, there is no need to solve the boundary layer cause a significant reduction of the mesh size and the computational domainA.2. Usually first grid cell needs to be $30 < y^+ < 300$. Use high-Re model like Standard $k - \epsilon$ and $RNG\ k - \epsilon$ and is used when you are more interested in the mixing rather than the forces on the wall.

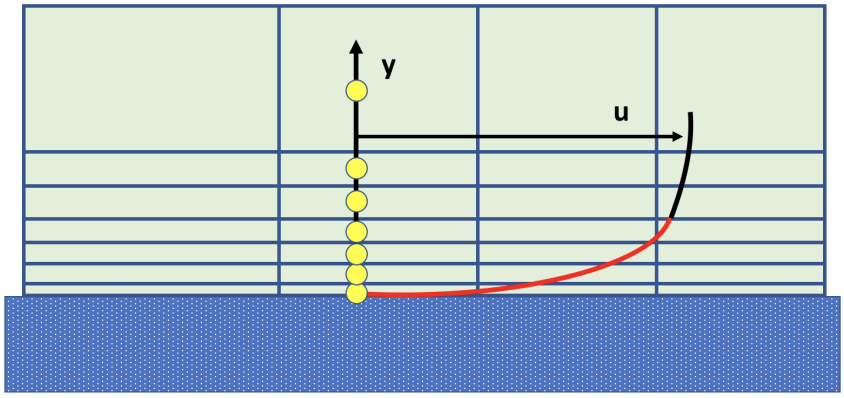

Figure A.1: Viscous sublayer resolving approach to resolve boundary layer (in red)

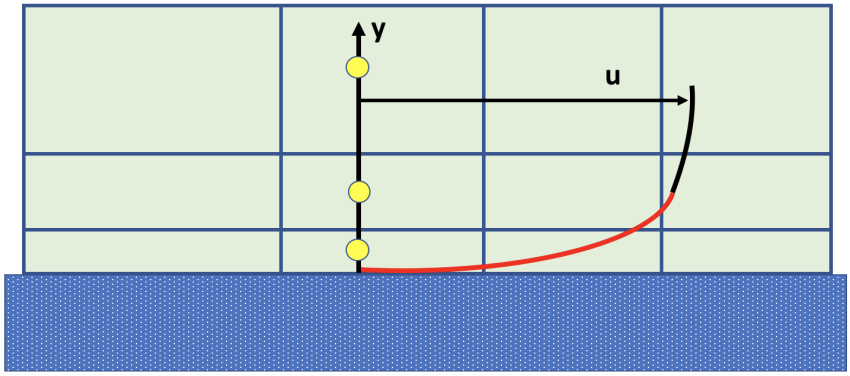

Figure A.2: Logarithmic-based Wall functions to resolve boundary layer (in red)

A.2 Wall Functions

The wall functions are based on the universal law of the wall, which basically states that the velocity distribution near to a wall is similar for almost all turbulent flows. The most important parameter when judging the applicability

of wall functions is the so-called dimensionless wall distance y^+ [9] denoted by:

$$y^+ = \frac{yu_\tau}{\nu} \tag{A.1}$$

- u_τ is the so called friction velocity
- y is the absolute distance from the wall
- ν is the kinematic viscosity

As the y^+ can be interpreted as a local Reynolds number, its magnitude can be expected to determine the relative importance of viscous and turbulent processes. Figure below A.3 shows the fractional contributions to the total stress of viscous and Reynolds stresses in the near wall region of channel flow.

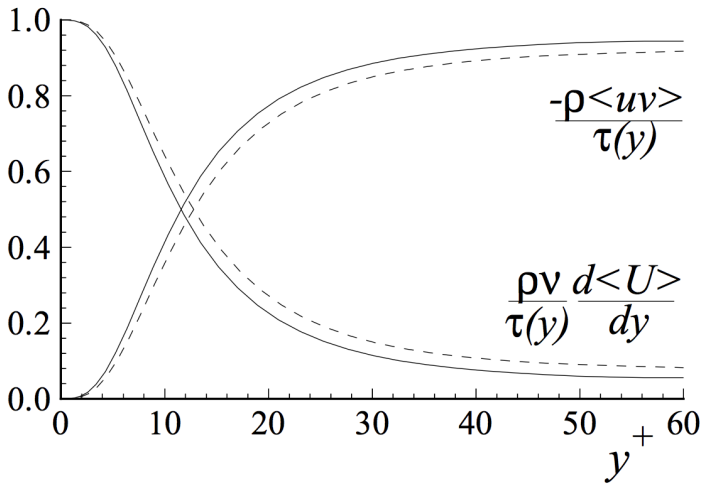

Figure A.3: Profiles of fractional contributions of the viscous and Reynolds stresses to the total stress. Dashed lines, Re = 5,600; solid lines, Re = 13,750 [9]

It can easily see that if we are in the viscous wall region with a $y^+ < 50$, there is a direct effect given by the viscosity on the shear stress. Opposite in the outer layer with $y^+ > 50$, the effect of viscosity is negligible.

At last, let's briefly introduce the friction velocity u_τ. It should be evident that the wall shear stress τ_w and the viscosity ν are important parameters.

$$u_\tau = \sqrt{\frac{\tau_w}{\rho}} \tag{A.2}$$

With

$$\tau_w = \rho\nu\left(\frac{d < U >}{dy}\right)_{y=0} \tag{A.3}$$

The dimensionless velocity is given by

$$u^+ = \frac{u}{u_{tau}} \tag{A.4}$$

A.3 Wall regions and layers

1. **The viscous sublayer** ($y^+ < 5$) In the viscous layer, the viscous effect dominate the fluid, so we can assume that the Reynolds shear stress is negligible. The "linear velocity law" is given by:

$$u^+ = y^+ \tag{A.5}$$

2. **The logarithmic area** ($y^+ > 30$) In the logarithmic layer, the flow is dominated by the turbulence stress and velocity profile varies very slowly with a logarithmic function alongside the distance y. Formula A.6 describes this region with the Karman constant κ of 0.41 and the constant $B = 5.2$.

$$u^+ = \frac{1}{\kappa} ln(y^+) + B \tag{A.6}$$

3. **The Buffer layer** ($5 < y^+ < 30$) The buffer layer is the transition region between the region dominate by viscosity and turbulence-dominated part

of the flow. Viscous and turbulent stresses have similar magnitude and since it is complex, the velocity profile is not well defined and the original wall functions avoid the first cell center located in this region.

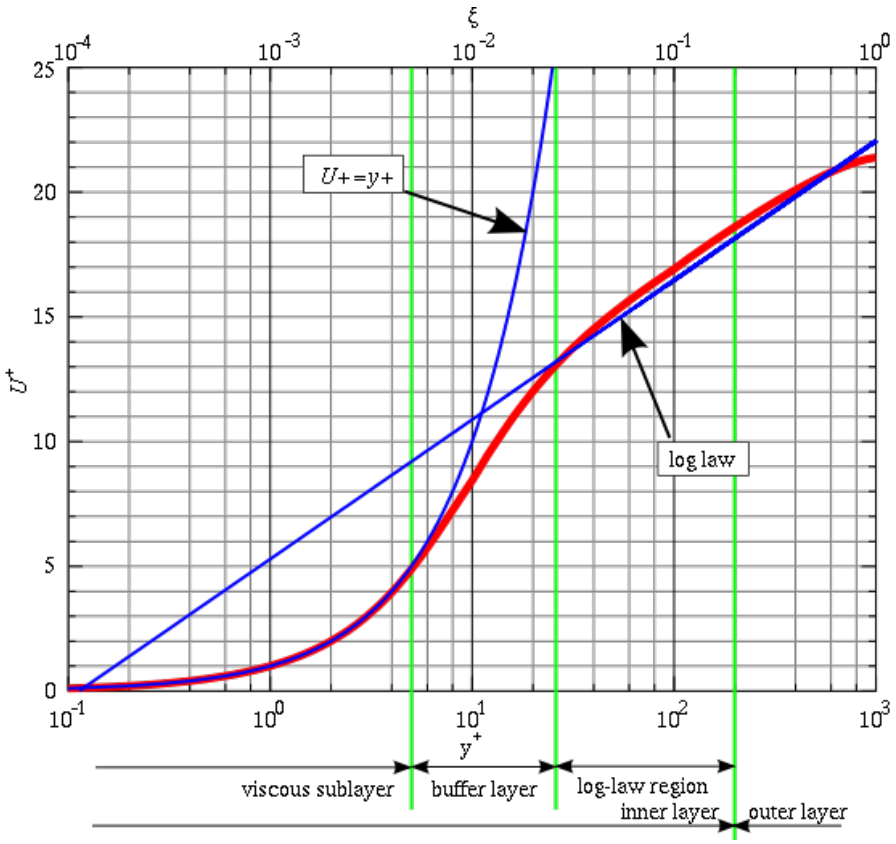

Figure A.4: The law of wall [9]

Bibliography

[1] Renato Tognaccini. *Lezioni di Aerodinamica dell'ala rotante.*
Federico II Napoli, 2008-2009 .

[2] Wayne Johnson. *Helicopter Theory.*
Dover Publications Inc, September 1st, 1980.

[3] Patankar SV. *Heat and mass transfer in turbulent boundary layers.*
Imperial College, London University, 1967.

[4] F. Moukalled L.Mangani M. Darwish. *The Finite Volume Method in Computational Fluid Dynamics.*
Springer, 2016.

[5] Milovan Peric Gerhard Jensen Heinz Herwig. *Development and Application of a Finite Volume Method for the Computation of Flows Around Moving Bodies on Unstructured, Overlapping Grids.*
Technische Universit¨at Hamburg-Harburg, 2005.

[6] ENAC. *Mezzi aerei a pilotaggio remoto.*
ENAC, 2018.

[7] E. Torenbeek. *Synthesis Of Subsonic Aircraft Design.*
Kluwer Academic Publisher, 1982.

[8] G. Guglieri. *Introduzione alla meccanica del volo.*
Celid, 2005.

[9] S. M. Salim, S.C. Cheah. *Wall y+ Strategy for Dealing with Wall-bounded Turbulent Flows.*
IMECS, 2009.

[10] ApcProp. *https://www.apcprop.com/.*

Acknowledgments

First of all I want to thank Professor Maggiore Paolo for his help in finding a company in which to carry out a thesis in this field and for his continuous support every time I went to his office.
In addition to Eng. Zamboni Fabio I want to thank you for taking the time to review my work, for being my tutor and sometimes a professional consultant.
I am really grateful to Larocca Francesco and D'Ambrosio Domenic for their suggestions and their time and for accepting my work.
To Melissa and my friends I want to say thank you for being my support and for putting up with me over the years.
Last but not least, I must say thank you to my parents to whom this thesis is dedicated, because without them and their help I would not be here and I would not be the boy I am now.

Thanks to everyone in my life for being by my side so far and from now on.